Bertola, N.J. and Smith, I.F.C. "A methodology for measurement-system design combining information from static and dynamic excitations for bridge load testing" J of Sound and Vibration, 463, 2019, 114953, https://doi.org/10.1016/j.jsv.2019.114953

A methodology for measurement-system design combining information from static and dynamic excitations for bridge load testing

Numa J. Bertola[1,2]

Ian F.C. Smith [1,2]

Abstract

Managing infrastructure assets is challenging for developed countries because of demand for increases in capacity, the scarcity of economic and environmental resources as well as ageing. Due to conservative approaches to construction design and practice, infrastructure often has hidden reserve capacity and its estimation may improve asset-management decisions. Static and dynamic bridge load testing has the potential to support engineers in their evaluation of infrastructure reserve capacity if monitoring data are associated with a robust structural-identification methodology. As choices of sensor types and locations directly influence structural-identification outcomes, sensor-placement methodologies have recently been developed to ensure successful model-updating results. Due to the nature of static and dynamic measurements, sensor-placement methodologies are usually developed independently. However, both types of load testing are used to update the same bridge behavior model. Therefore, when sensor-placement strategies are established independently, redundant sensor information is likely. In this study, two measurement-system design methodologies are proposed. First, a new methodology for sensor-placement for dynamic load testing is presented, where expected information gain of natural frequencies is used to prioritize sensor-location selections. Then, a measurement-system-design methodology combining information of both static and dynamic load testing is proposed. Finally, the methodology is evaluated using a full-scale bridge. A well-designed measurement system based on expected information gain enhances system identification and reserve-capacity estimation.

Keywords:

Structural identification; error-domain model falsification; optimal sensor placement; joint entropy; modal identification; effective independence method.

[1] ETH Zurich, Future Cities Laboratory, Singapore-ETH Centre, 1 CREATE Way, CREATE Tower, 138602 Singapore.

[2] EPFL, Applied Computing and Mechanics Laboratory, CH-1015 Lausanne, Switzerland; E-mail: numa.bertola@epfl.ch.

1 Introduction

The annual global expenditure of the construction industry represents more than $10 trillion [1]. Accounting for 40% of this total, civil infrastructure must be managed efficiently. Due to safe design and construction practices, infrastructure often has reserve capacity that is well above the margins created by safety factors in code requirements. However, accurate reserve-capacity assessment is challenging because of uncertainties in material, geometry and boundary conditions. Measurement data, collected through monitoring, has the potential to support engineers for reserve-capacity assessment.

Structural identification involves interpreting field measurements to improve knowledge of structural behavior [2]. Although model-free strategies may successfully detect damage and perform behavior interpolation [3], a model-based approach must be used when extrapolation is needed, such as when infrastructure reserve-capacity is assessed [4].

In such cases, field measurements are carried out and the data are used to improve model-prediction accuracy. Due to the use of complex behavior models, for instance finite-element (FE) models, numerous assumptions are required and this leads to several sources of uncertainties. Traditional approaches to structural identification, such as residual minimization and Bayesian model updating, usually assume that uncertainties have zero-mean Gaussian forms [5]–[7]. Since structural models are designed to be safe, the zero-mean assumption is not satisfied in this context [8]. Furthermore, the estimation of prediction-error correlations between sensor locations is challenging as usually, little information is available [9]. Although modifications to traditional implementations of Bayesian model updating are possible, they lead to complex system-identification formulations [10], [11]. Introduced by Goulet and Smith [12], error-domain model falsification (EDMF) is an easy-to-use structural-identification approach. Compared with traditional Bayesian updating, EDMF provides more accurate (albeit less precise) model-parameter identification since it represents explicitly systematic uncertainties in a way that is compatible with practical engineering knowledge [13]. Recently, EDMF has been applied to full-scale case studies to assess the reserve-capacity and to evaluate the worst-case load capacity [14], [15].

Structural-identification outcomes are directly dependent on the design of the measurement system. Surprisingly, sensor types and positions are typically chosen using only qualitative rules of thumb arising from engineering experience. Quantitative studies on optimal sensor placement have been recently carried out to maximize the information gain by sensor configurations for both static and dynamic load tests [16], [17].

Although load testing is often used for identification, static and dynamic load tests can provide unique information. Information may also be redundant [18]. Due to their nature, measurement systems for static and dynamic tests are typically designed independently. Measurement-system-design methodologies should involve information from static and dynamic tests simultaneously in order to maximize the total expected information gain.

For both static and dynamic tests, finding the optimal sensor configuration is usually formulated as a simple optimization task. The computational complexity of the sensor-placement algorithm is exponential with respect to the number of sensors [19]. Although global-search optimization algorithms have been proposed [20], most researchers have preferred to use sequential searches (greedy algorithms) to reduce the computational effort when there are more than a few sensors [21].

Several approaches, such as either minimizing the information entropy in posterior model-parameter distributions [22], [23] or maximizing information entropy in multiple-model predictions [24], [25] have been developed to evaluate sensor locations in terms of their performance for model-parameter estimations. Most authors have disregarded the mutual information between sensor locations, leading to sensor clustering issues [26]. Furthermore, a constant uncertainty level at all locations is assumed.

Once first sensor locations are selected, Papadimitriou and Lombaert [27] included the effect of spatially-correlated prediction errors, thus reducing information-entropy values of neighboring sensors and thus avoiding sensor clusters. Papadopoulou et al. [28] introduced a methodology involving a hierarchical algorithm to examine potential locations. Mutual information between sensor locations was explicitly accounted for in an objective function that maximized the joint entropy. This sensor placement algorithm, combining a hierarchical algorithm with joint-entropy maximization, explicitly incorporated systematic uncertainties and was successfully applied to sensor-placement studies for wind-around-building sensor placement [29]. The methodology has later been adapted for structural identification in order to account for several sensor types and a modification was proposed to include mutual information between several static load-test configurations [30].

As these strategies required uncertainty-distribution quantification to evaluate possible sensor locations, these need engineers to provide input information. For dynamic tests, some researchers preferred to use only modal information, such as mode-shape vectors, to identify optimal sensor locations, mostly based on the Fisher Information Matrix (FIM) [31]. Several sensor-placement objective functions for modal identification have been proposed, for instance, modal kinetic energy (MKE) [32], effective independence method (EFI) [33], modal assurance criterion (MAC) [34], QR-decomposition [35] and mutual information [36]. Relations between these objective functions have been explored [37]. Several studies compared these objective functions in terms of information gain and for lattice structures [38], timber-frame structures [39] and bridges [40]. These last studies concluded that the EFI method is the best sensor-placement objective function for modal identification. In the EFI method, each mode shape is assumed to have the same performance on structural identification. However, some case studies showed that this assumption is incorrect [19], [41] because information gained on model parameters and modelling errors may differ significantly between mode shapes.

This paper contains a description of a measurement-system-design methodology for dynamic load testing using expected information from natural frequencies to prioritize sensor-location selections using the EFI method. Although not directly linked to sensor locations, the expected performance of mode-shapes is assessed using natural-frequency predictions. Once the expected information gain by each mode shape is quantified, sensor-location selections in EFI are prioritized to improve the identification of useful mode shapes for model updating without requiring estimation of mode-shape-vector uncertainties. Then, measurement-system-design methodologies for dynamic and static load testing are combined to minimize the redundant information gain between measurement systems. Finally, a full-scale case study is used to evaluate this approach. The novelty of this paper lies in the prioritization of the mode-shape identification in the EFI method using the expected information gain of natural frequencies. Additionally, this approach proposed a combination of measurement-system-design methodologies for static and dynamic load testing in order to minimize the redundancy in information gain between them.

The study is organized as follows. Background methodologies are shown in Section 2. Section 3 includes a description of the methodology for measurement-system design using expected information from dynamic load testing in the EDMF framework. Section 4 shows how this information is combined with the static load testing for the first time in a measurement-system design methodology. A full-scale case study is described in Section 5 with optimal measurement-system results presented in Section 5.4 for dynamic load testing and in Section 5.5 for both static and dynamic load testing.

2 Background

In this section, background methodologies that have been developed previously are presented. First, the structural-identification methodology, called error-domain model falsification, is presented in Section 2.1. After this, the sensor-placement algorithm for static measurements, called hierarchical algorithm, is described in Section 2.2.

2.1 Structural identification – Error-domain model falsification

Error-domain model falsification (EDMF) is a recently developed methodology for structural identification [12]. Finite-element (FE) model predictions are compared with field measurements in order to identify plausible model instances of a parameterized model class. A model instance is generated by assigning a unique combination of parameter values to a model class, which consists of a FE parametric model including characteristics such as material properties, geometry, boundary conditions and excitations.

Model predictions at location i, $g_i(\mathbf{\Theta})$ are generated by assigning a vector of parameter values $\mathbf{\Theta}$ to the selected model class. Assuming R_i to be the real response of a structure—unknown in practice— and $\hat{y}_i$ to be the measured value at a sensor location i among n_y monitored locations, model uncertainty $U_{i,g}$ and the measurement uncertainty $U_{i,y}$ are first estimated and then connected to the real behavior using the following equation:

$$g_i(\mathbf{\Theta}) + U_{i,g} = R_i = \hat{y}_i + U_{i,\hat{y}} \; \forall i \in \{1, \dots, n_y\} \quad (1)$$

Following [42], modeling and measurement uncertainties are combined in a unique source $U_{i,c}$ using Monte-Carlo simulations and Eq. (1) is transformed in Eq. (2). The residual r_i presents the difference between the model prediction and the field measurement at a sensor location i.

$$g_i(\mathbf{\Theta}) - \hat{y}_i = U_{i,c} = r_i \quad (2)$$

In the EDMF implementation, the identification process starts with the generation of an initial model set (IMS) that consists of n_Ω instances $\Omega = \{\mathbf{\Theta}_1, \dots, \mathbf{\Theta}_{n_\Omega}\}$. EDMF selects plausible model instances by falsifying those for which residuals exceed threshold bounds given combined uncertainties and a target reliability of identification, which is typically fixed at 95% [12]. Model instances with residuals that do not exceed threshold bounds at each sensor location are included in the candidate model set (CMS). The set of candidate models is defined to be those models satisfying the inequalities in using Eq. (3).

$$\Omega'' = \{\mathbf{\Theta} \in \Omega'' | \forall i \in \{1, \dots, n_y\} \; u_{i,low} \leq r_i \leq u_{i,high}\} \quad (3)$$

where Ω'' is the candidate model set (CMS) built of model instances that have not been falsified. The thresholds, $u_{i,low}$ and $u_{i,high}$, represent lower and upper bounds expressing the shortest intervals through the probability density function (PDF) of combined uncertainties $f_{U_i}(u_i)$ at a measurement location i, including a probability of identification ϕ^{1/n_y}. The Šidák correction $1/n_y$ [43] maintains a constant level of confidence when multiple sensor measurements are compared with model-instance predictions (Eq. (4)).

$$\forall i = 1, \dots, n_y: \phi^{1/n_y} = \int_{u_{i,low}}^{u_{i,high}} f_{U_i}(u_i) du_i \quad (4)$$

Since little information is usually available to describe the combined-uncertainty distribution, candidate models are set to be equally likely [44]. Thus, they are assigned an equal probability as expressed in Eq. (5).

$$\Pr(\mathbf{\Theta} \in \Omega'') = \frac{1}{\int \theta \in \Omega'' \mathrm{d}\theta} \quad (5)$$

Falsified model instances are assigned a null probability (Eq. (6)).

$$\Pr(\mathbf{\Theta} \notin \Omega'') = 0 \quad (6)$$

Consequently $\mathbf{\Theta}''$, is the vector of random variables describing the realistic model-parameter values of candidate model instances given field measurements. Its PDF is defined using Eq. (7).

$$f_{\mathbf{\Theta}''} = \begin{cases} \frac{1}{\int \theta \in \Omega'' \mathrm{d}\theta}, & if\ \mathbf{\Theta} \in \Omega'' \\ 0 & , otherwise \end{cases} \quad (7)$$

If all initial model instances are falsified, the entire model class is falsified ($\Omega'' = \emptyset$). This means that no model instance is compatible with sensor measurements given combined uncertainties. This result is usually an indication of incorrect assumptions in the model-class definition [45]. This particular situation highlights an important advantage of EDMF compared with residual minimization. In such cases, EDMF results lead to a re-evaluation of assumptions and a new model class is generated, avoiding wrong parameter identification.

2.2 Sensor-placement algorithm – Hierarchical algorithm

Prior to measuring a structure, a sensor-placement strategy has the potential to identify optimal measurement systems when a limited knowledge of model-parameter values is available. Once the numerical model is built and the model class is selected, prediction data from a population of model instances are generated. A set of model predictions is a typical input to evaluate the expected information gain by sensor locations, such as prediction variability.

The information entropy, from information theory, was introduced as a sensor-placement objective function for system identification [22]. At each sensor location i, the range of model-instance predictions is divided into $N_{I,i}$ intervals, where the interval width W_i is constant. W_i is equal to the difference between upper and lower bounds of the combined source of uncertainty $U_{i,c}$. The probability that the model-instance prediction $g_{i,j}$ falls inside the jth interval equals to $P(g_{i,j}) = m_{i,j}/N_{MI}$, where $m_{i,j}$ is the number of model instances falling inside the jth interval, and N_{MI} is the total numer of model instances. At a sensor location i, the information entropy $H(g_i)$ is evaluated using Eq. (8).

$$H(g_i) = -\sum_{j=1}^{N_{I,i}} P(g_{i,j}) \log_2 P(g_{i,j}) \qquad (8)$$

Papadopoulou et al. [28] proposed the joint entropy as a new sensor-placement objective function to quantify the redundancy of information gain between sensor locations. The joint entropy $H(g_{i,i+1})$ assesses the information entropy between sets of predictions, taking into account the mutual information between them. For a set of two sensors, it is defined using Eq. (9).

$$H(g_{i,i+1}) = -\sum_{k=1}^{N_{I,i+1}} \sum_{j=1}^{N_{I,i}} P(g_{i,j}, g_{i+1,k}) \log_2 P(g_{i,j}, g_{i+1,k}) \qquad (9)$$

where $k \in \{1, \dots, N_{I,i+1}\}$ and $N_{I,i+1}$ is the maximum number of prediction intervals at the i+1 location and $i+1 \in \{1, \dots, n_s\}$ with the number of potential sensor locations n_s. An alternative form expresses the joint entropy to be equal to the sum of the individual information entropies of sets of predictions minus the mutual information between sensor i and i+1 $I(g_{i,i+1})$ as presented in Eq. (10).

$$H(g_{i,i+1}) = H(g_i) + H(g_{i+1}) - I(g_{i,i+1}) \qquad (10)$$

$I(g_{i,i+1})$ is unknown in practice and can be calculated only if individual information entropies and the joint entropy of sensor locations i and i+1 are known. The hierarchical algorithm [28] is a sequential algorithm (greedy search). Therefore, the sensor-location selection is not reevaluated in its subsequent selections. At each iteration, the hierarchical algorithm re-evaluates the joint-entropy objective function of remaining sensor locations and selects the location with the largest value. The algorithm stops when all sensor locations are selected.

Bertola et al. [30] proposed a modification of the hierarchical algorithm to take into account mutual information between static load tests based on joint entropy. For a sensor location i and model predictions of two static load tests, the joint entropy evaluation is described in Eq. (11), in which $j \in \{1, \dots, N_{I,i_l}\}$ and N_{I,i_l} is the maximum number of intervals at the location i associated with a load test l, $k \in \{1, \dots, N_{I,i_{l+1}}\}$ and $N_{I,i_{l+1}}$ is the maximum number of intervals at the location i associated with another load test $\mathrm{l}+1 \in \{1, \dots, n_{LT}\}$ with the number of potential load tests n_{LT}. The hierarchical algorithm is able to evaluate the expected information gained by a measurement system, consisting of a sensor configuration and a set of load tests.

$$H(g_{i_l,i_{l+1}}) = -\sum_{k=1}^{N_{I,i_{l+1}}} \sum_{j=1}^{N_{I,i_l}} P(g_{i_l,j}, g_{i_{l+1},k}) \log_2 P(g_{i_l,j}, g_{i_{l+1},k}) \quad (11)$$

3 Measurement-system-design methodology for dynamic load testing

In this section, the methodology for sensor-placement for dynamic load testing is developed. Figure 1 presents the steps of the methodology. The methodology is divided into four phases. Each phase is presented in a subsection below. First, the task of measurement-system design is defined such as the model-class, selection, the generation of model-instance predictions or the engineering decisions (Section 3.1). The expected information gain of each natural frequency is assessed to determine the optimal number of natural frequencies for falsification (Section 3.2). This phase involves the identification of the most useful modes for structural identification. However, natural-frequency predictions are not directly linked to a sensor location. Therefore, the next phase involves using a sensor-placement strategy to rank sensor locations (Section 3.3). To take advantage of the information gained in the second phase, the sensor-placement strategy prioritizes locations that help identify useful modes for falsification. Finally, Section 3.4 presents information-gain metrics that are used to define the optimal sensor configuration. These metrics help evaluate the number of sensors required to identify accurately natural frequencies of the most useful modes.

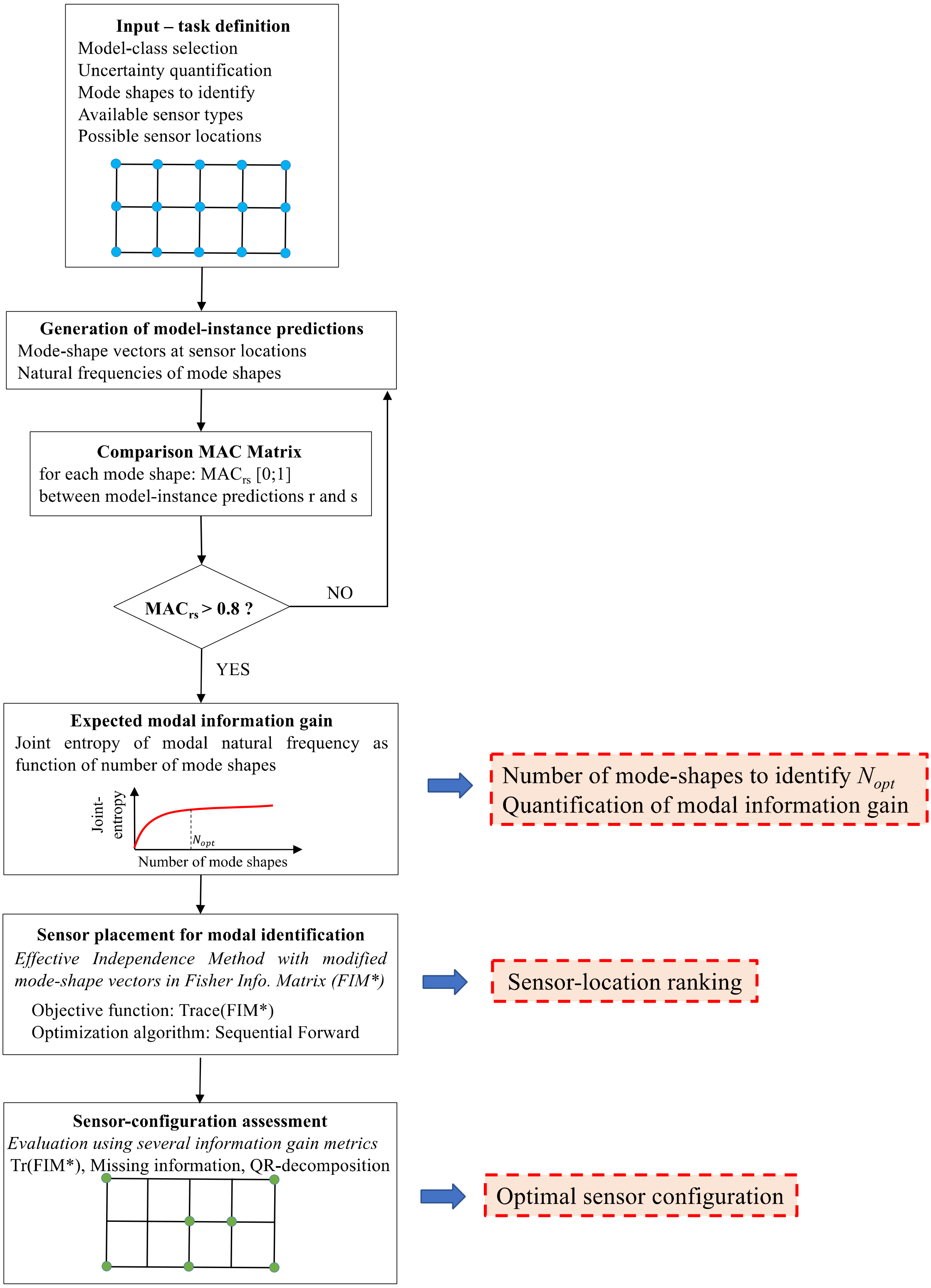

Figure 1 Measurement-system-design methodology for dynamic load tests.

3.1 Task definition

Before assessing sensor locations, several steps are required. This section describes important steps in the definition of the sensor-placement task definition. The first step is to define the input information. The finite-element model of the structure is built to obtain reliable quantitative predictions of measurable variables such as mode-shape vectors at each possible sensor location. Engineers choose sensor types and the number of sensors available in the study and select possible locations. The number of mode shapes is estimated using engineering judgement, signal-to-noise ratio evaluation and the maximum number of available sensors.

Model parameters, which have the highest impact on predictions, are selected using a sensitivity analysis. Due to geometrical and mathematical simplifications of the numerical model, significant non-parametric uncertainties are always involved. Model uncertainties must be estimated because the expected information-gain assessment of natural frequencies is influenced by them (Section 3.2).

Multiple model instances are generated using a sampling technique to obtain a discrete population of model-parameter values within plausible ranges. For each model instance, typical outputs are mode-shape vectors at each sensor location and a natural frequency for each mode shape. Then, for each mode shape, a population of model predictions is generated. Model instances constitute the initial model set, which is the dataset used in the sensor-placement strategy to rank possible sensor locations (Section 3.2).

The last step of the task-definition phase involves evaluating if model-instance predictions for each mode shape are compatible. By compatible, it is assumed that mode-shape vectors φ between two model instances r and s have a modal assurance criterion (MAC) larger or equal to 0.8 (Eq. (12)) [34].

$$\mathrm{MAC_{rs}} = \frac{\left(\varphi_r^T \varphi_s\right)^2}{(\varphi_r^T \varphi_r)(\varphi_s^T \varphi_s)} \geq 0.8 \qquad (12)$$

This condition ensures that model instances are comparable in terms of predictions. While this condition is typically fulfilled [46], it may happen that the appearance order of mode-shapes is inversed since model-parameter values influence natural-frequency values.

3.2 Assessment of natural-frequency expected information gain

The expected information gained by natural frequencies can be assessed using the joint entropy in a similar way to Section 2.2 for static measurements. In this case, the output variable g_m is the natural-frequency predictions of the mode m and is not related to sensor locations.

Following Eq. (8) to (10), the expected information gain of sets of natural-frequency predictions can be quantified.

The joint-entropy assessment provides two features to the sensor-placement strategy (Section 3.3). First, a subset of useful mode shapes can be selected by removing mode shapes that do not significantly contribute to the joint entropy. Then, an estimation of the contribution of each mode shape can be assessed through the joint-entropy increase when the mode shape is added to the subset. Figure 2 presents a sketch of typical joint-entropy evaluation as function of number of mode shapes. Natural frequencies are ranked by expected information gain. The joint entropy increases until it reaches a maximum value, corresponding to the maximum expected information gain by dynamic load testing. In this example, mode shapes selected after the 8th position do not provide useful additional information as the joint entropy does not increase significantly. Therefore, only $N_{opt,2}$ mode shapes only are identified. Similarly, another asset manager may decide to only use $N_{opt,1}$ modes that correspond to 90% of the maximum joint entropy to reduce the number of sensors to install on the bridge and therefore reduce the cost of the monitoring. The information provided by each mode shape can be quantified in a similar way by assessing the increase of joint entropy when the mode shape m is added to the system.

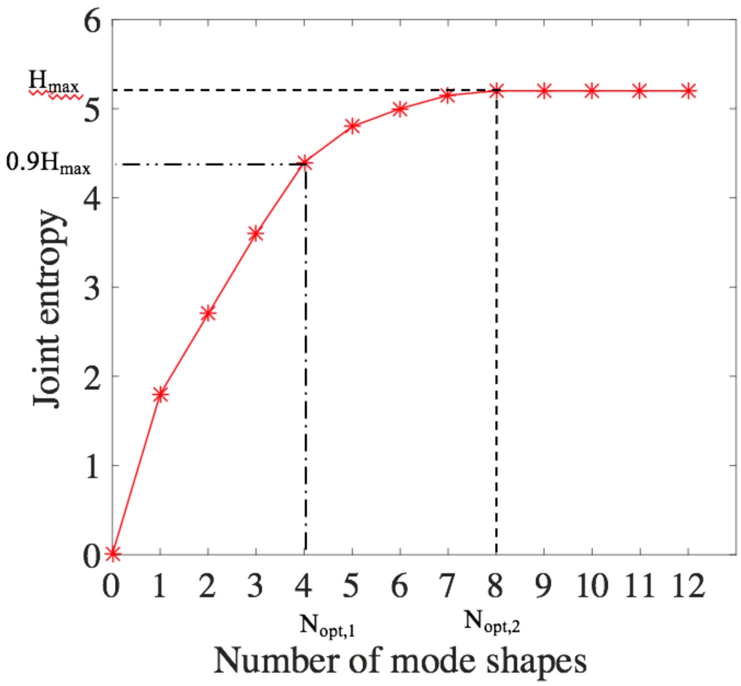

Figure 2 Sketch of the joint entropy of natural frequencies as function of number of mode shapes.

3.3 Modified effective independence method for modal identification

3.3.1 Equations of motion

Any sensor-placement methodology for modal identification starts with the equation of motion for a linear structural system. Using n degree of freedom (DOFs) is formulated in Eq. (13) as function of time t.

$$\mathbf{M}\ddot{\mathbf{u}}(\mathrm{t}) + \mathbf{C}\dot{\mathbf{u}}(\mathrm{t}) + \mathbf{K}\mathbf{u}(\mathrm{t}) = \mathbf{F}(\mathrm{t}) \tag{13}$$

where $\mathbf{u}(\mathrm{t}) \in [\mathrm{n} \times 1]$ is the vector of displacement responses, $\mathbf{M}, \mathbf{C}$ and $\mathbf{K} \in [\mathrm{n} \times \mathrm{n}]$ are the mass, damping and stiffness matrices respectively, and $\mathbf{F}(\mathrm{t}) \in [\mathrm{n} \times 1]$ is the vector of excitations. A typical assumption is that the structural system is characterized by proportional damping [39]. Eq. (14) can be rewritten in Eq. (15).

$$\ddot{\boldsymbol{\xi}}(\mathrm{t}) + \bar{\mathbf{C}}\dot{\boldsymbol{\xi}}(\mathrm{t}) + \boldsymbol{\Lambda}\boldsymbol{\xi}(\mathrm{t}) = \boldsymbol{\Phi}^{\mathbf{T}}\mathbf{F}(\mathrm{t}) \tag{14}$$

With

$$\boldsymbol{\Lambda} = \mathrm{diag}\{\omega_1^2, \ldots, \omega_n^2\} \in [n \times n] \tag{15}$$

$$\bar{\mathbf{C}} = \mathrm{diag}\{2\zeta\omega_1, \ldots, 2\zeta\omega_n\} \in [n \times n] \tag{16}$$

where $\boldsymbol{\xi}(t) \in [n \times 1]$ is the vector of modal coordinates, ω_j is the j^{th} natural frequency, ζ_j designates the j^{th} modal damping ratio, $\boldsymbol{\Phi} \in [n \times n]$ is the matrix of mode shapes, $\boldsymbol{\Lambda}$ is the matrix of natural frequencies and $\bar{\mathbf{C}}$ is the modified damping matrix. Moreover, the matrix of mode shapes may be $\boldsymbol{\Phi} \in [m \times m]$ if a subset of m < n mode shapes are involved. The structural response in the original coordinate space is thus: $\mathbf{u}(t) = \boldsymbol{\Phi}\xi(t)$.

3.3.2 Traditional effective independence method

The aim of a sensor-placement methodology for modal identification is to build the best estimate of the structural response $\boldsymbol{\xi}(\mathrm{t})$. This implies the minimization of the covariance matrix of the estimated errors. Following [31], maximizing the Fisher Information Matrix (FIM) would lead to the minimization of the covariance matrix and thus to the best estimate of $\boldsymbol{\xi}(\mathrm{t})$. The FIM $\mathbf{Q} \in [n \times n]$ is computed using Eq. (17) in which $\mathbf{L} \in [\mathrm{n} \times \mathrm{n}]$ is a Boolean matrix that maps the sensor locations to the DOFs. Figure 3 presents FIM calculation. The case of a simple oscillator with two possible sensor locations and two mode shapes is used for simplicity purposes. A numerical example is added to show the FIM calculation in Figure 3.

$$\mathbf{Q} = (\mathbf{L}\boldsymbol{\Phi})^{\mathrm{T}}(\mathbf{L}\boldsymbol{\Phi}) \tag{17}$$

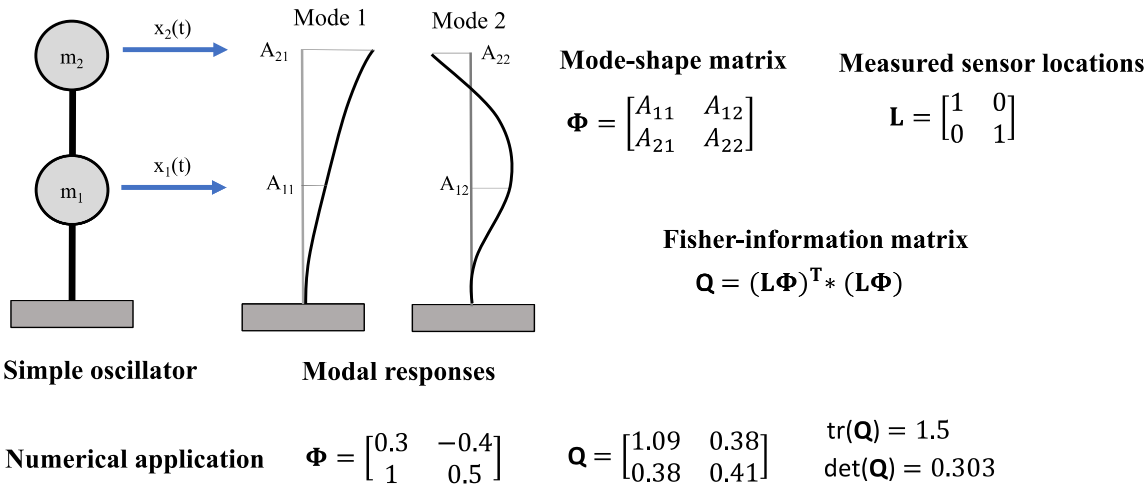

Figure 3 Fisher-information-matrix (FIM) calculation for the case of a simple oscillator with two sensor locations and two mode shapes.

The traditional effective independence method (EFI), introduced by Kammer [33], evaluates possible sensor locations through both the linear independence between target mode shapes and the intensity of measured value. Using a sequential sensor placement with Forward (FSSP) or Backward (BSSP) greedy strategies for sensor placement, sensor configurations are evaluated through FIM properties such as the trace, or the determinant. An important characteristic of the FIM is that the matrix is singular in the case of the number of sensors being lower than the number of mode shapes. In such situations, the FIM determinant cannot be used as an objective function for sensor placement.

An important assumption of the traditional EFI method is that each mode is equally useful for the model-parameter identification. If this assumption is correct, each natural frequency should have the same influence on the model falsification. However, several case studies show that this assumption is incorrect [19], [41] as the variability of frequency predictions is significantly influenced by the model parameters to identify. The next section describes how the EFI method is modified to take into account the importance of mode shapes for falsification in the sensor-location ranking.

3.3.3 Modified effective independence method

A solution proposed by others, for example [16], [23], involves using parameter uncertainties and a Bayesian framework to identify sensor locations that will reduce the posterior distribution of model parameters. This proposal necessitates evaluations of the combined uncertainty $U_{i,c}$

for mode-shape vectors. Such recommendations are currently missing in the literature due to difficulties associated with uncertainties of mode shapes.

The strategy proposed in this study is to use the information provided during the modal expected information gain (Section 3.2) to weight mode-shape vectors according to the expected information that they provide. Each column in the mode-shape matrix $\mathbf{\Phi}$, corresponding to mode-shape m, is therefore adjusted according to its contribution in the joint-entropy evaluation. The contribution is estimated as the difference of joint entropy ΔH_m when the mode shape m is added to the system. Therefore, an importance Boolean matrix $\mathbf{I_{mp}} \in [\mathrm{n} \times \mathrm{n}]$ is added to the FIM calculation, in which $I_{mp_{m,m}} = \Delta \mathrm{H}_m$. $\mathbf{I_{mp}}$ will thus prioritize sensor locations in the EFI method.

The assessment of the modal-frequency joint entropy does not involve sensor locations. In order to accurately measure natural frequencies, possible sensor locations must be able to reconstruct accurately the mode shapes. A simple example is the following. If a local mode shape is involved and possible sensor locations are not present in the specific area, it is not possible to identify this mode shape and it should not be involved in the sensor placement. Therefore, a second identifiability Boolean matrix $\mathbf{I_{nt}} \in [\mathrm{n} \times \mathrm{n}]$ is added to the FIM calculation where the identifiability of each mode shape is a ratio between the maximum deformation of the mode shape m at possible sensor locations, $A_{L,max}$, divided by the global maximum deformation of this mode shape, A_{max}. As both amplitude values are influenced by model predictions, mean predictions are used. For a mode shape m, the identifiability matrix is calculated as $\mathrm{I_{nt}}_{\mathrm{m,m}} = \mathrm{mean}(A_{L,max_{\mathrm{m}}}(\boldsymbol{\theta}))/\mathrm{mean}(A_{max_m}(\boldsymbol{\theta}))$ and is bounded between 0 and 1.

Mode-shape vectors are influenced by modal parameters to identify. As mode-shape vectors of model instances are comparable (Section 3.1), the average value of mode-shape vectors is taken as an approximation. The modified mode-shape vector for modal identification is presented in Eq. (18).

$$\overline{\mathbf{\Phi}} = \mathbf{\Phi}\left(\mathrm{mean}\left(\mathrm{g_i}(\boldsymbol{\theta})\right)\right) \cdot \mathbf{I_{mp}}\mathbf{I_{nt}} \quad (18)$$

The modified FIM can be calculated using Eq. (19). Figure 4 presents steps of the calculation of the modified FIM for a simple oscillator, where the importance-factor and identifiability matrices are used to weigh the mode-shape matrix $\mathbf{\Phi}$. When compared with the traditional FIM calculation (Figure 3), the modified FIM calculation involves the expected performance in terms of information gain of mode-shape vectors. In the numerical example, the value of joint entropy of the second mode shape is small, showing a smaller importance of this mode for model parameter identification. By including the importance matrix, FIM properties such as the trace are then reduced; i.e. $\mathrm{tr}(\bar{\mathbf{Q}})$ equals to 1.18, while $\mathrm{tr}(\mathbf{Q})$ equals to 1.5 in Figure 3 when no important matrices are taken into account. This result shows that sensor locations useful to identify the second mode shape such as A_1 will not have priority since this mode does not contribute significantly to the information gain.

$$\bar{\mathbf{Q}} = (\mathbf{L}\bar{\mathbf{\Phi}})^{\mathrm{T}}(\mathbf{L}\bar{\mathbf{\Phi}}) \quad (19)$$

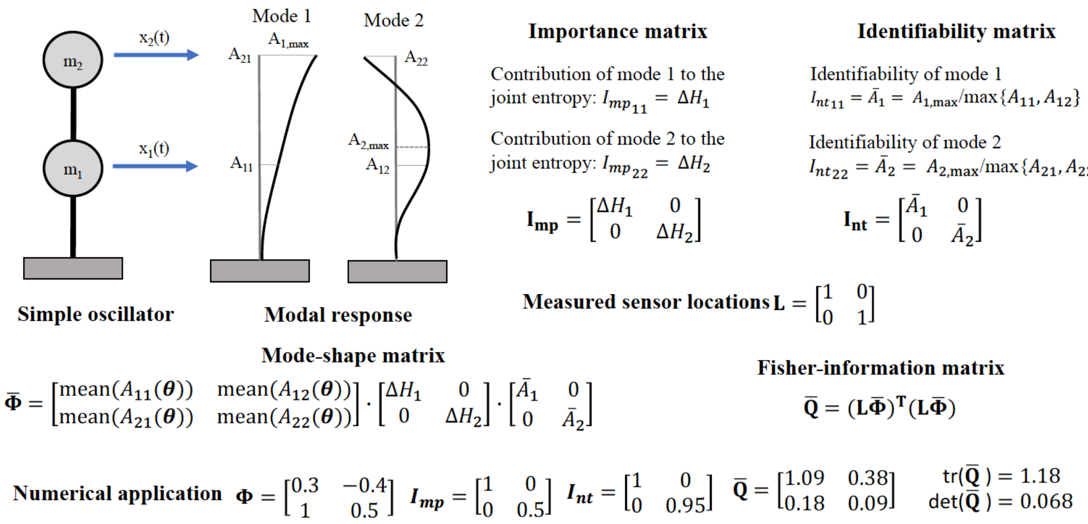

Figure 4 Modified Fisher-information matrix (FIM) calculation using the simple-oscillator case and joint-entropy evaluations of mode shapes.

Since the number of sensors involved in this study is low, the trace of $\bar{\mathbf{Q}}$ is used as an objective function for sensor placement. The determinant of $\bar{\mathbf{Q}}$ is equal to zero in cases where number of sensors is lower than the number of mode shapes needing identification. Additionally, a sequential forward (FSSP) is used as an optimization strategy, following [21].

3.4 Information-gain metrics for modal identification

Once the objective function for the sensor placement and the optimization algorithm are selected, sensor locations are ranked. To define the optimal sensor configuration, quantification of information gain metrics must be carried out. In this section, a strategy involving two metrics is proposed to evaluate sensor configurations in terms of their ability to reconstruct mode shapes. The missing information and QR decomposition are shown to be complementary. Information-gain metrics and are presented in Sections 3.4.1 and 3.4.2.

3.4.1 Missing information

The first metric, called missing information *MI*, represents a comparison the information provided by a sensor configuration k with the maximum information that can be gained if the sensor configuration includes all possible sensor locations. The metric, inspired by the mutual-information objective function introduced by Stephan [36], compares the FIM of a sensor configuration k $\bar{\mathbf{Q}}_k$ with the FIM of the sensor configuration K including all possible sensor locations $\bar{\mathbf{Q}}_K$. This metric is calculated using Eq. (20). When MI tends to zero, the maximum possible information gain, represented by sensor configuration K, is obtained by the sensor configuration k. A non-zero value of MI means that adding sensors to the sensor configuration will provide more information. Therefore, the information-gain metric MI must be minimized.

$$\mathrm{MI}(k) = \frac{\|\bar{\mathrm{Q}}_\mathrm{k} - \bar{\mathrm{Q}}_\mathrm{K}\|}{\|\bar{\mathrm{Q}}_\mathrm{k} + \bar{\mathrm{Q}}_\mathrm{K}\|} \in [0,1] \tag{20}$$

3.4.2 QR decomposition

The second information-gain metric, called QR decomposition (QRD), provides an evaluation of the linear independence of mode-shape vectors. The term QR comes from the decomposition of a matrix A into the product A = QR, where Q is an orthogonal matrix and R an upper diagonal matrix. Introduced by Schedlinski and Link [35], the metric uses rows of the mode-shape matrix $\mathbf{\Phi}$ instead of columns used in EFI. For N_m modes, the linear independence of each pair of rows $\langle \psi_n, \psi_m \rangle \in [1xn]$ is evaluated using Eq. (21). The matric $\mathbf{LI} \in [N_m \; x \; N_m]$ is therefore a triangular matrix, in which the $LI_{n,m}$ is equal to zero if mode-shape vectors n and m are perfectly orthogonal and equal to one if they are linearly dependent. The information-gain metric *QRD* sums $\mathrm{LI}_{\mathrm{n,m}}$ elements of a sensor configuration k (Eq. (22)). When *QRD* tends to zero, all pairs of mode-shape vectors are orthogonal and therefore, each mode shape is distinguished. Non-zero values signify that some mode shapes cannot be differentiated and, therefore, adding sensors to the configuration can convey additional information in terms of the linear independence of mode-shape vectors. Therefore, the information-gain metric *QRD* must be minimized.

$$\mathrm{LI}_{\mathrm{n,m}} = \frac{(\psi_n^T \psi_m)^2}{(\psi_n^T \psi_n)(\psi_m^T \psi_m)} \tag{21}$$

$$\mathrm{QRD}_\mathrm{k} = \sum_\mathrm{i}^{\mathrm{Nm}} \sum_\mathrm{j}^{\mathrm{Nm}} \mathrm{LI}_{\mathrm{i,j}} \tag{22}$$

4 Methodology for measurement system design combining information from static and dynamic testing

In order to monitor a structure, engineers may perform dynamic and static tests. Both tests differ in terms of the nature of the data collected (time-series data for dynamic tests and single measurements at sensor locations for static tests) and numerical models for predictions. Nevertheless, information collected during monitoring are often used to update the same parameter values of the numerical behavior model. Therefore, sensor-placement methodologies should be combined in order to avoid redundant information gain between dynamic and static load testing. In this section, a methodology is proposed to design measurement systems that are intended for including static and dynamic load testing (Figure 5).

The strategy begins with the building of a numerical model of the structure. Primary parameters to identify are chosen and non-parametric uncertainties are estimated. The engineer then selects available sensor types and sensor locations for both static and dynamic tests. Additionally, possible static load tests are designed.

Once engineering decisions are made, model instances are generated for both static predictions, such as deflection at static-sensor locations for each static load test and dynamic predictions such as natural frequencies and mode-shape vectors at dynamic-sensor locations. In order to compare the information entropy of each type of measurement (i.e. static measurements and natural frequencies), an important limitation of the methodology is that both tests must use the same model class; the same dataset in terms of model-parameter values must be compared. In this situation, predictions of static measurements and natural frequencies of dynamic tests can be compared using the joint-entropy metric for information gain as presented in Section 3.2. Mathematical details are presented in Section 4.1.

The optimal sensor configuration for the static test is explicitly obtained from the joint-entropy assessment, following the methodology presented in Section 2.2. Concerning the optimal sensor configuration for dynamic test, Sections 3.3 and 3.4 must still be performed. However, the importance matrix $\mathbf{I_{mp}}$ is adapted from the joint-entropy assessment using both static and dynamic tests, while the identifiability matrix $\mathbf{I_{nt}}$ remains unchanged as the same possible dynamic-sensor locations are used. When these steps are completed, the optimal sensor configuration for dynamic testing is found.

4.1 Joint-entropy assessment

The information provided by static measurements and natural frequencies, which in this section are called measurements, is assessed the same way as in Sections 2.2 and 3.2. In this situation, the output variable, g, is either the natural-frequency predictions of the mode m or the static predictions at sensor location, i, such as deflection. Following Eq. (8) to (10), the expected information gain of sets of natural-frequency predictions can be quantified.

The expected information gain provided by each measurement can be quantified using the joint-entropy assessment. This result makes two contributions to the sensor-placement strategies. First, useful static measurements are directly found and thus, the optimal static sensor configuration is revealed. Secondly, useful mode shapes and their information-gain quantification are provided for the sensor-placement strategy for modal identification as presented in Section 3, where the importance factor of each mode shape is evaluated using the joint-entropy assessment combining static and dynamic testing.

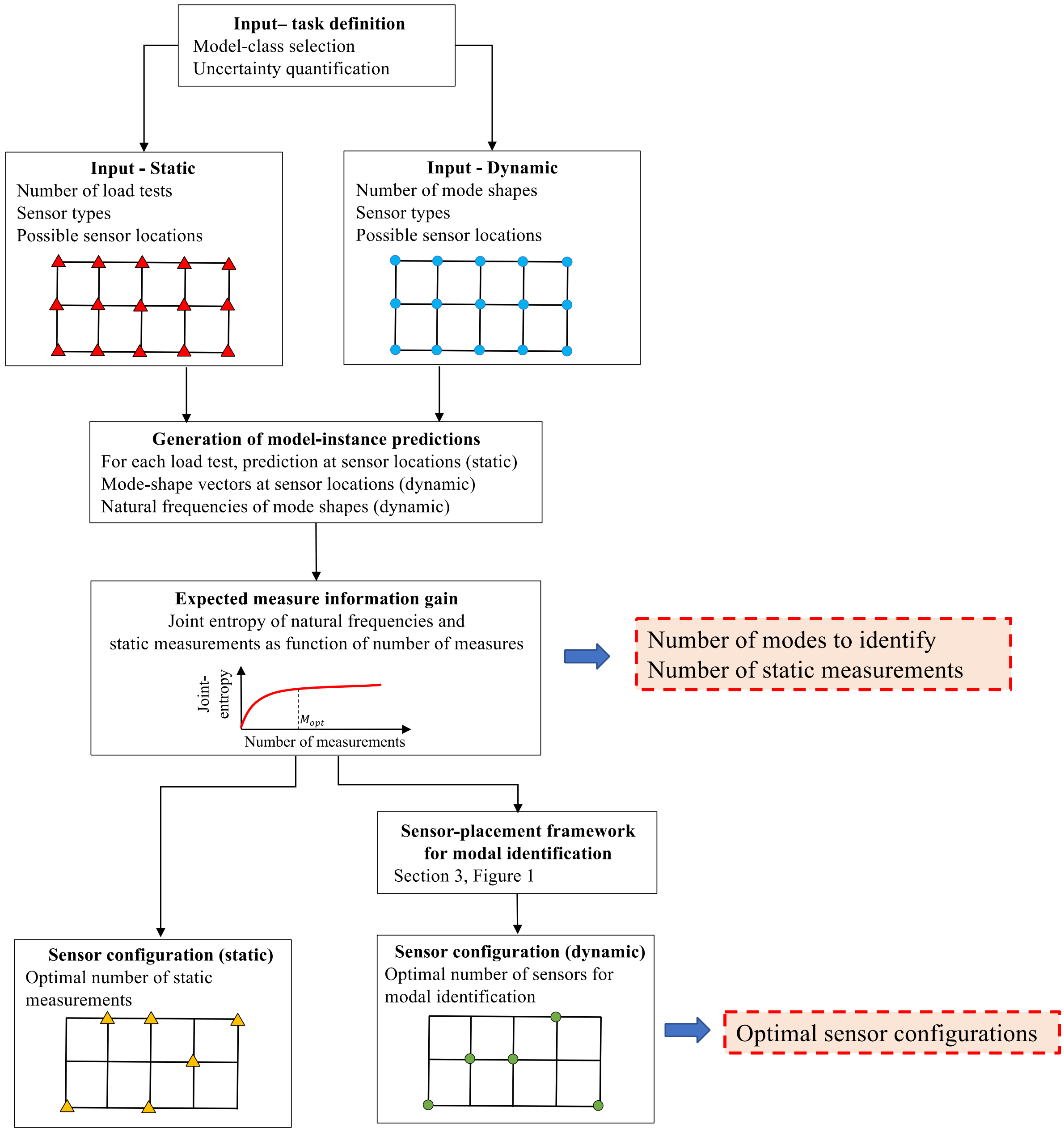

Figure 5 Measurement-system-design methodology combining information from static and dynamic load testing.

5 Case study

Engineering details of the full-scale case study are presented in Section 5.1. Sections 5.2 and 5.3 show the selection of the model class and of the mode shapes. Optimal measurement systems are presented in Section 5.4 for dynamic load testing and in Section 5.5 for both static and dynamic load testing.

5.1 Bridge presentation

The full-scale case study is a 32-year-old bridge in Singapore. The pre-stressed pre-cast concrete structure has four beams carrying three unidirectional traffic lanes over a simply-supported span of 32 meters. Principal characteristics of the bridge are presented in Figure 6 including the static load test and possible sensor locations. Sensor locations were chosen based on engineering judgement and signal-to-noise-ratio estimation. As this sensor configuration could not been modified, this study focuses on evaluating the performance of selected sensor locations.

For the static load test, sensors included two inclinometers (I_i) on the south parapet and four deflection targets (P_i) on the girders (Figure 6: A; B). A laser tracker was positioned on the road below the bridge and was used to measure deflections at target locations. To monitor the dynamic behavior of the bridge, 10 accelerometers were installed on parapets (Figure 6: A). Eight free-vibration tests were carried out on the bridge using a single truck at several speeds. Additionally, ambient-vibration measurements were recorded during 15 minutes when no truck was running. Additional information concerning the monitoring is presented in [47].

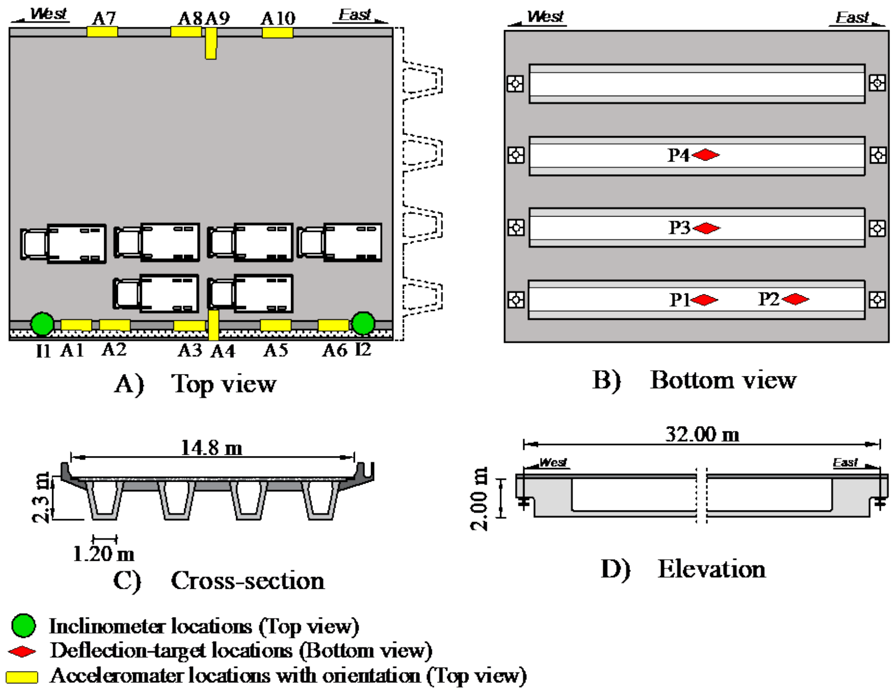

Figure 6 Bridge geometry showing sensor locations and the static load test: A) Top view; B) Bottom view; C) Cross-section; D) Elevation.

5.2 Model-class selection

The selection of the model class is an important step of structural identification, where primary parameters are chosen and uncertainties are estimated. Four model parameters have the largest influence on model predictions: the Young modulus of the concrete E_{con}; the density of the concrete ρ_{con}; the rotational stiffness of the bearing devices K_{rot}; and the vertical stiffness of the bearing devices K_{lon}. Plausible ranges of model-parameter values are estimated using engineering judgement and are presented in Table 1. Non-structural elements, such as the asphalt pavement, are included in the numerical model to reduce model-simplification uncertainties.

Table 1 Model-parameter initial ranges for structural identification.

Primary parameters	Symbol	Initial ranges
Equivalent Young's modulus of concrete beams and deck (GPa)	E_{con}	[20 – 42]
Concrete equivalent density (kg/m^3)	ρ_{con}	[1800 – 3000]
Rotational stiffness of bearing devices (log(Nmm/rad))	K_{rot}	[9 – 13]
Vertical stiffness of bearing devices (log(N/mm))	K_{long}	[8 – 11]

Table 2 presents the upper and lower bounds of model-class uncertainties and measurement uncertainties. Measurement uncertainties include the sensor precision based on manufacturing specifications and site conditions, the measurement repeatability that is usually estimated by conducting multiple series of tests on site, and the influence of the sensor installation. Model-class uncertainties are estimated using engineering judgement, technical literature, and local knowledge. Since a limited number of parameters can be sampled to generate the initial model set, an additional uncertainty source estimated using stochastic simulation is included.

Table 2 Estimations of model and measurement uncertainties.

Uncertainty source	**Displacements – (P)**		**Rotations – (I)**		**Accelerometer – (S)**	
	Min	Max	Min	Max	Min	Max
Model simplifications (%)	-5	13	-5	13	-8	5
Mesh refinement (%)	-1	1	-1	1	0	2
Additional uncertainty (%)	-1	1	-1	1	-1	1
Sensor precision	-0.05 mm	0.05 mm	-1 µrad	1 µrad	-0.1 Hz	0.1 Hz
Repeatability	-0.15 mm	0.15 mm	-4 µrad	4 µrad	-0.05 Hz	0.05 Hz
Sensor installation (%)	-	-	-5	5	-2	2

5.3 Mode-shape selection

The eight first mode shapes are selected for the modal identification based on global behavior and low natural-frequency values (Figure 7). Within this 4-parameter space, 1,000 initial model instances were generated using Latin Hypercube Sampling (LHS). Model-instance predictions consist of deflection and inclination measurements for the static load testing (Figure 6) and the natural frequency of each mode shape and the mode-shape vector at each possible accelerometer location.

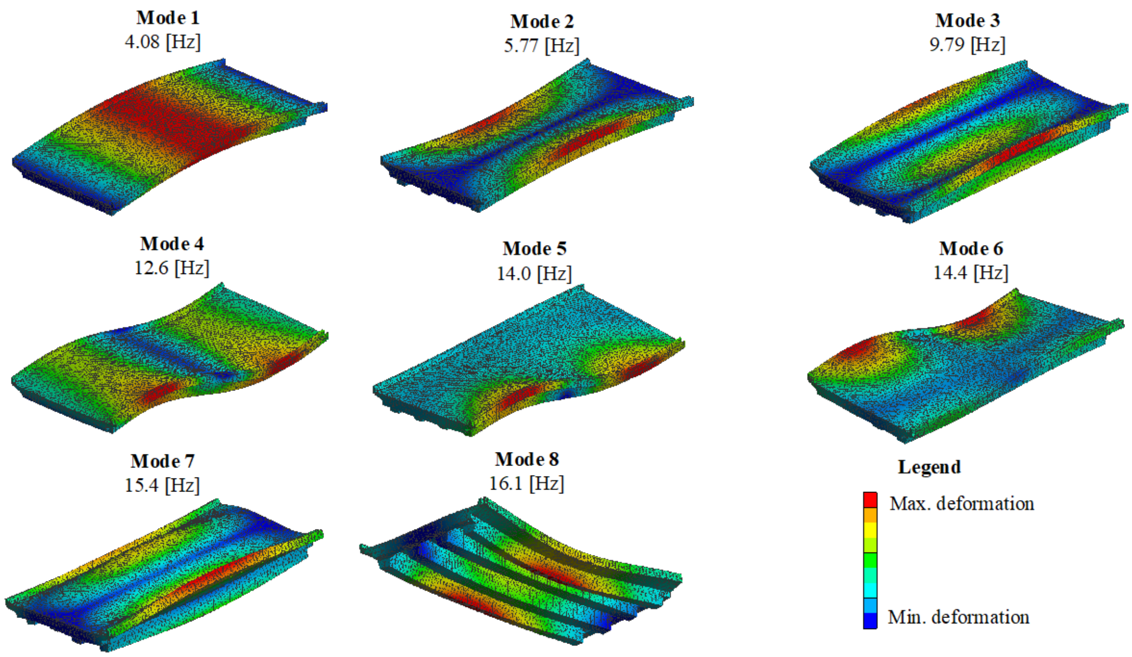

Figure 7 Visualization of mode shapes with their respective mean natural frequency.

Before designing a measurement system, the comparability of model-instance predictions for each mode shape must be checked, following Section 3.1. Figure 8 presents the distribution of MAC values between model instances r and s for respectively, mode 1 (Figure 8A), mode 2 (Figure 8B), mode 4 (Figure 8C) and mode 7 (Figure 8D). Horizontal axes are scaled between the minimum values of MAC_{rs} and 1. Following Eq. (12), MAC_{rs} must be above 0.8. For all mode shapes, this condition is satisfied and thus, the model-instance generation is validated. Additionally, as the values in the distribution are almost equal to 1, this means that model instances do not significantly influence the shape of the mode but more the amplitude. Therefore, the implicit assumption of Eq. (18), taking the mean value as a good approximation of the modal behavior, is reasonable.

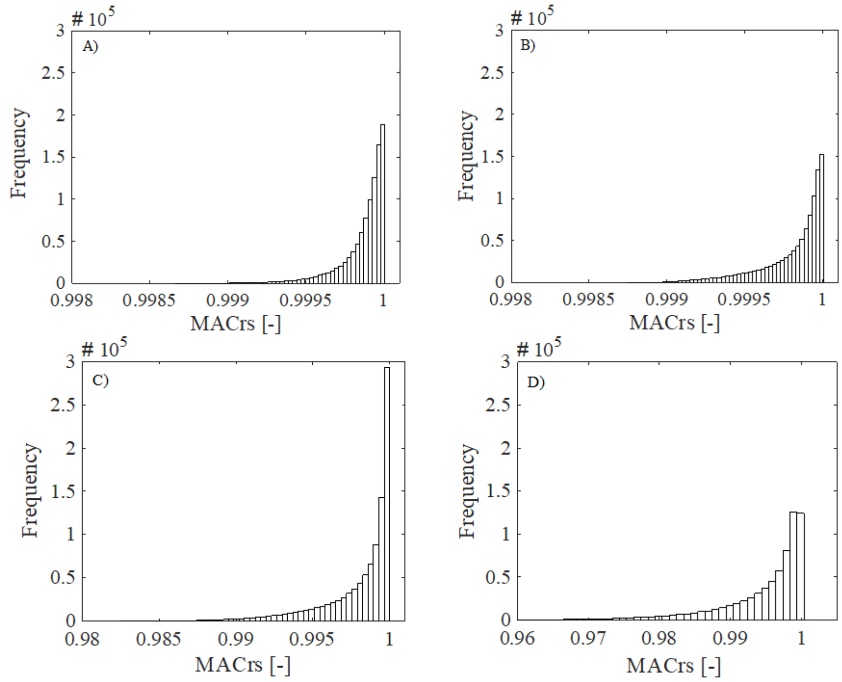

Figure 8 Modal assurance criterion (MAC) for model instances i and j for specific modes. A) mode 1; B) mode 2; C) mode 4; D) mode 7.

5.4 Measurement-system design for dynamic load testing

In this subsection, the methodology presented in Section 3 for sensor placement for dynamic load testing is applied to the Singapore case study. First, the mode-shape joint entropy is assessed in Section 5.4.1. Then, the addition of the importance matrix and identifiability matrix to the FIM calculation is compared with the traditional approach in Section 5.4.2.

5.4.1 Joint-entropy assessment of natural-frequency expected information gain

This section contains an assessment of the expected information gain of natural-frequency predictions of the eight mode shapes presented in Section 5.3. The information entropy is presented in Figure 9A, showing the expected information gain of each mode shape independently. Each mode shape displays similar performance with information-entropy values between 1.28 and 1.62, meaning they have close expected performance for structural identification as the information entropy is bounded between 0 and 10. Mode shape 1 shows a slightly larger information entropy and will be selected as the best mode shape in the first iteration of the hierarchical algorithm (Section 2.2). Figure 9B presents the joint entropy evaluation of mode-shape sets as function of number of mode shapes. The joint entropy increases significantly with first mode shapes (M1, M6, M7, M4) added to the set and then, the expected information gain is limited. Although mode 1 is selected in the first position, subsequent mode-shape selections do not follow the mode-shape order. Higher mode shapes, such as modes 6 and 7, have more additional information when mode 1 is already involved. As each mode shape increases the joint entropy evaluation, each mode shape provides unique information. Therefore, all mode shapes will be involved in the measurement-system design for modal identification (Section 5.4.2).

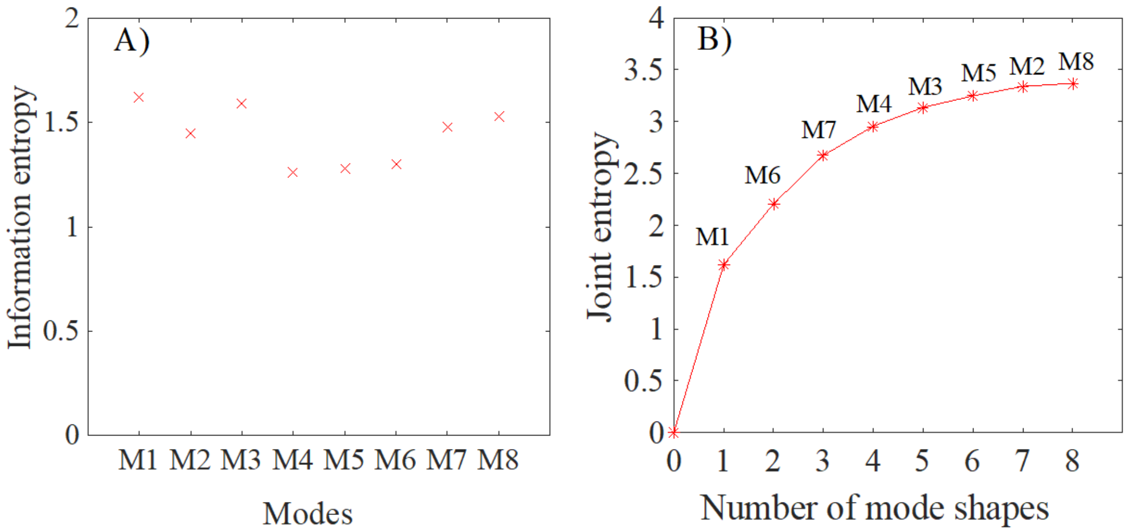

Figure 9 A) Information entropy (Eq. (8)) of natural frequencies of mode shapes; B) Joint entropy (Eq. (9)) of the natural frequency of mode-shape set as function of the number of modes.

5.4.2 Sensor-placement for modal identification

In this section, the sensor placement based on modal identification is performed. In order to justify the proposition to modify the mode-shape vectors using importance-factor and identifiability matrices (Eq. (18)), several importance-factor scenarios will be compared. Table 3 presents five scenarios that are compared as well as equal importance factors in terms of objective-function evaluation (Section 5.4.2.1), sensor-location ranking (Section 5.4.2.2) and information-gain metrics (Section 5.4.2.3). The first importance-factor scenario $\mathbf{I}_{\mathbf{mp,1}}$ includes only an importance matrix based on the information-entropy results (Figure 9A), as introduced in Section 3.3.3. The second importance-factor scenario $\mathbf{I}_{\mathbf{mp,2}}$ uses only the joint entropy as importance factors based on results of Figure 9B. As redundancy of information gain inevitably occurs, the mode-1 result is corrected using Eq. (10) and the information entropy of the first two mode shapes is selected. The third importance-factor scenario is the identifiability matrix $\mathbf{I}_{\mathbf{nt}}$, as introduced in Section 3.3.3. The fourth and fifth importance-factor scenarios take into account both importance-factor and identifiability matrices using the information entropy $\mathbf{I}_{mp,1}*\mathbf{I}_{nt}$ and the joint entropy $\mathbf{I}_{mp,2}*\mathbf{I}_{nt}$ respectively.

Table 3 Mode-shape-vector importance factors.

Modes	**Mode-shape-vector importance-factor scenarios**				
	Information entropy (IE) [-] $\mathbf{I}_{mp,1}$	Joint entropy gain (JE) [-] $\mathbf{I}_{mp,2}$	Identifiability (ID) [-] $\mathbf{I}_{nt}$	IE and ID [-] $\mathbf{I}_{mp,1}*\mathbf{I}_{nt}$	JE and ID [-] $\mathbf{I}_{mp,2}*\mathbf{I}_{nt}$
1	1.62	0.91	0.98	1.57	0.89
2	1.45	0.09	0.91	1.33	0.08
3	1.59	0.18	0.87	1.38	0.16
4	1.29	0.28	0.28	0.35	0.08
5	1.28	0.11	0.83	1.06	0.09
6	1.30	0.62	0.53	0.69	0.33
7	1.48	0.46	0.45	0.67	0.21
8	1.53	0.03	0.51	0.78	0.02

5.4.2.1 Objective-function evaluation

For each importance-factor scenario, the objective-function evaluation (trace of the modified FIM $\overline{\mathbf{Q}}$) is presented in Figure 10 with respect to the number of sensors. In order to compare the importance-factor scenarios, results are normalized using the maximum objective-function evaluation of each importance-factor scenario $\widehat{\mathrm{tr}}(\overline{\mathbf{Q}})$. For all importance-factor scenarios, the objective function reaches a near-maximum value from the 8th sensor added to the sensor configuration. This shows that more than eight sensors provide no new information. For any number of sensors, scenario $\mathbf{I}_{mp,2}$ and $\mathbf{I}_{mp,2}*\mathbf{I}_{nt}$ outperform other importance-factor scenarios. This result is validated using information-gain metrics (Section 5.4.2.3).

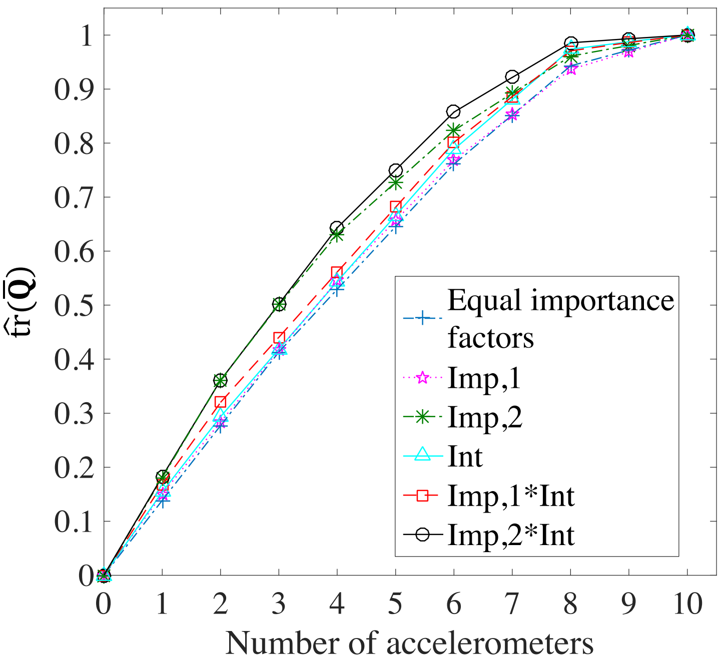

Figure 10 Normalized trace of modified Fisher Information Matrix ($\bar{\mathbf{Q}}$) for scenarios as function of number of sensors.

5.4.2.2 Sensor-location ranking

In this section, the sensor-location ranking for each importance-factor scenario is presented. Figure 11 shows the first five sensor locations selected for each importance-factor scenario. Globally, sensor locations 3, 7, 8 and 10 have the largest expected information gain as they are selected in first positions in most of importance-factor scenarios. Additionally, from the first sensor selected, the importance-factor scenario $\mathbf{I_{mp,1}}$*$\mathbf{I_{nt}}$ differs in terms of sensor configuration. This shows that the modification of the FIM influence sensor-location evaluations to prioritize the identification of useful mode shapes for structural identification. This result explains the difference in terms of objective-function evaluations (Figure 10) but must be validated using information-gain metrics (Section 5.4.2.3).

A)	Equal importance factors				
Sensor	Number of sensors in sensor config.				
selected	1	2	3	4	5
A1					
A2				•	•
A3					
A4					
A5					•
A6					
A7	•	•	•	•	•
A8			•	•	•
A9					
A10		•	•	•	•

B)	$I_{mp,1}$				
Sensor	Number of sensors in sensor config.				
selected	1	2	3	4	5
A1					
A2					•
A3				•	•
A4					
A5					
A6					
A7		•	•	•	•
A8	•	•	•	•	•
A9					
A10			•	•	•

C)	$I_{mp,2}$				
Sensor	Number of sensors in sensor config.				
selected	1	2	3	4	5
A1					
A2					
A3				•	•
A4					
A5					•
A6					
A7	•	•	•	•	•
A8			•	•	•
A9					
A10		•	•	•	•

D)	I_{nt}				
Sensor	Number of sensors in sensor config.				
selected	1	2	3	4	5
A1					
A2			•	•	•
A3		•	•	•	•
A4					
A5				•	•
A6					
A7					•
A8	•	•	•	•	•
A9					
A10					

E)	$I_{mp,1}$ * I_{nt}				
Sensor	Number of sensors in sensor config.				
selected	1	2	3	4	5
A1					
A2					•
A3		•	•	•	•
A4					
A5					
A6					
A7			•	•	•
A8	•	•	•	•	•
A9					
A10				•	•

F)	$I_{mp,2}$ * I_{nt}				
Sensor	Number of sensors in sensor config.				
selected	1	2	3	4	5
A1					
A2					
A3	•	•	•	•	•
A4					
A5					•
A6					
A7			•	•	•
A8		•	•	•	•
A9					
A10				•	•

Figure 11 Accelerometer-location (Ai) ranking for importance-factor scenarios presented in Table 3.A) Equal importance factors B) information entropy $\mathbf{I_{mp,1}}$ only; C) Joint entropy $\mathbf{I_{mp,2}}$ only; D) Identifiability matrix only $\mathbf{I_{nt}}$; E) Information entropy and identifiability matrix $\mathbf{I_{mp,1}*I_{nt}}$; F) Joint entropy and identifiability matrix $\mathbf{I_{mp,2}*I_{nt}}$.

5.4.2.3 Information-gain metrics for modal identification

In this section, sensor configurations obtained with the importance-factor scenarios are compared using the two information-gain metrics introduced in Section 3.4. Figure 12 presents the missing information MI with respect to the number of accelerometers. Globally, as the missing information must be minimized, all importance-factor scenarios lead to an increase in information gain with the number of sensors. The traditional approach represented by the scenario with no importance factors is over-performed by all remaining scenarios, while the scenario $\mathbf{I_{mp,2}*I_{nt}}$ outperforms all remaining scenarios, indicating a higher information gain. Additionally, for this importance-factor scenario, the missing-information metric does not significantly decrease when six sensors are used in the sensor configuration, while the drop in missing information is negligible from eight sensors in the sensor configuration. Based on the missing information as an inverse information-gain metric for modal identification, 6 to 8 sensors are recommended in the sensor configuration. Next, results are validated using the second information-gain metric (QR-decomposition).

Figure 13 presents QR-decomposition information-gain metric (*QRD*) with respect to the number of accelerometers. The metric evaluates the linear independence between mode-shape vectors and must be minimized. Globally, all importance-factor scenarios lead to a decrease in

QRD with increasing number of sensors and they perform similarly on this information-gain metric. The QR-decomposition metric as an inverse information-gain metric for modal identification is almost constant between 5 to 8 sensors and shows a slight decrease when the 9th sensor is added to the sensor configuration. Therefore, for all importance-factor scenarios, a sensor configuration of 6 to 10 sensors is recommended. The scenario $\mathbf{I_{mp,2}*I_{nt}}$ performs as well as the equal-importance scenario. This shows that the prioritization of sensor-location selections to identify useful mode shapes for falsification does not affect significantly the ability to detect all mode shapes in the EFI method.

Regarding both information-gain metrics, the importance-factor scenario $\mathbf{I_{mp,2}*I_{nt}}$ outperforms other scenarios. Using the importance and identifiability matrices lead to a prioritization of sensor-location selections to identify useful mode shapes for falsification. This important-factor scenario outperforms the traditional approach for modal identification, when all mode shapes are assumed to have the same performance for structural identification. Additionally, a sensor configuration of 6 to 9 sensors is recommended for structural identification based only on dynamic load testing.

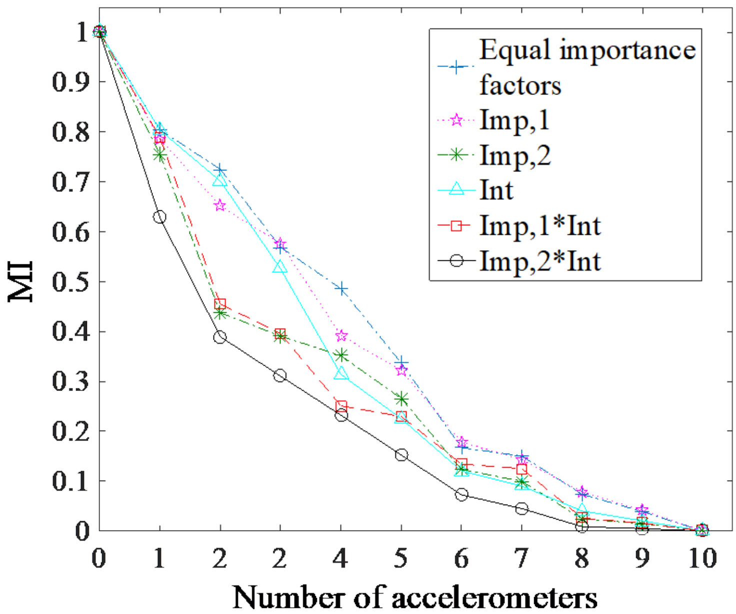

Figure 12 Missing-information metric (*MI*) for importance-factor scenarios as function of number of accelerometers.

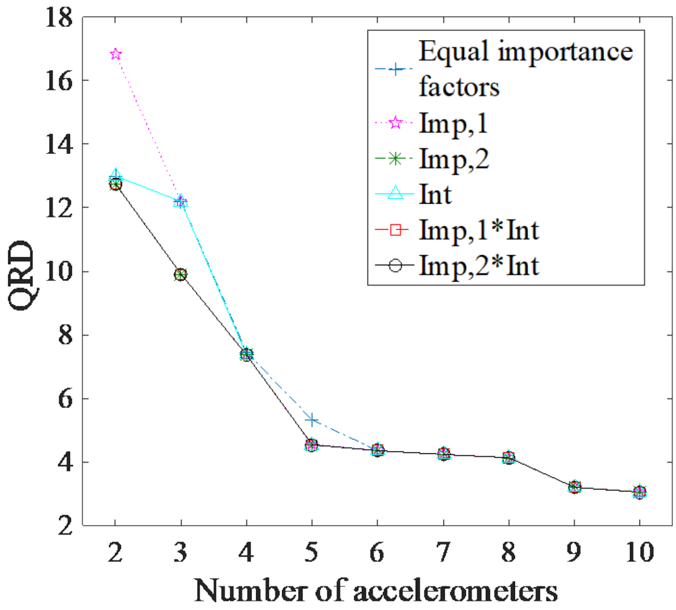

Figure 13 QR-decomposition metric (*QRD*) for importance-factor scenarios as function of number of accelerometers.

5.5 Measurement-system design including static and dynamic tests

In this subsection, the methodology presented in Section 4 for measurement-system design including information from static and dynamic tests is applied to the Singapore case study. First, the joint entropy of natural frequencies and static measurements is assessed in Section 5.5.1. Then, the sensor-placement methodology for modal identification is performed in Section 5.5.2 to design the optimal measurement system for dynamic tests.

5.5.1 Joint-entropy assessment of static measurements and natural frequencies

In this section, the expected information gain from both static (deflection and inclination) and dynamic (natural frequency) measurements is assessed using the joint entropy as presented in Section 4.1. Figure 14A presents the information entropy of both static and dynamic measurements. Globally, static measurements show larger information-entropy values than natural frequencies. The inclinometer I2 presents the largest information-entropy value and is therefore the best measurement if measurements are used individually. Additionally, two sensor types are used for static tests. Figure 14B presents the joint-entropy assessment of measurement sets. Using both static and dynamic measurements lead to significantly larger joint entropy values than using static or dynamic measurements individually for any number of measurements in the measurement set. This shows that both tests provide unique information and should be used for structural identification of this case. Multi-sensor types have been shown to reduce the mutual information between measurements [30]. The joint entropy of both tests increases for any measurements added to the measurement set. Each measurement provides useful additional information.

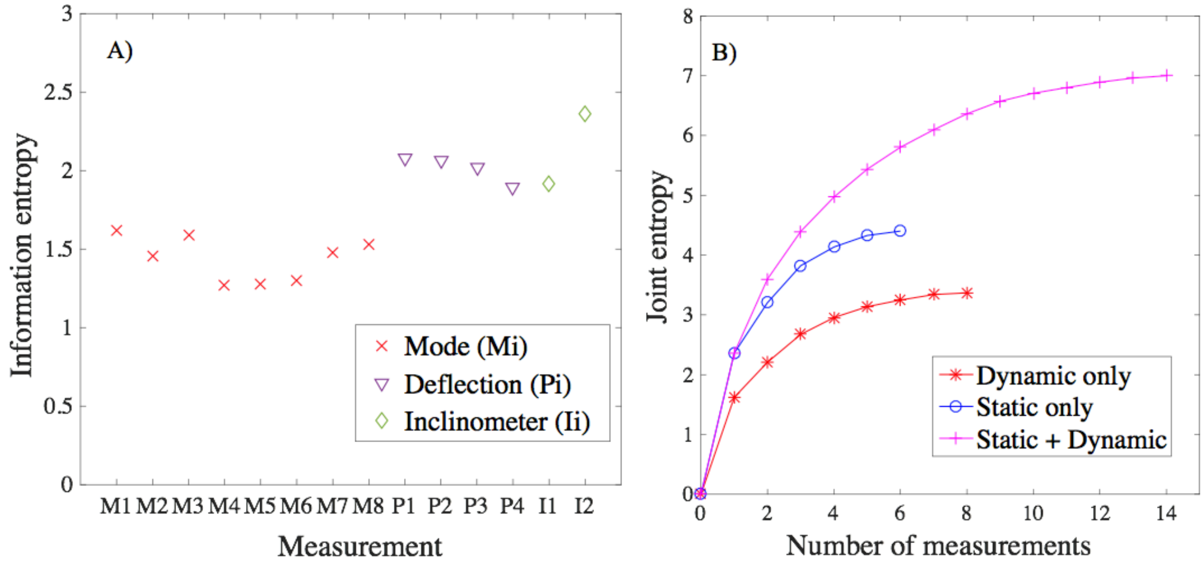

Figure 14 A) Information entropy of measurements; B) Joint entropy as function of number of measurements.

Figure 15 presents the measurement ranking from the joint-entropy assessment when both static and dynamic measurements are used. As shown using information-entropy evaluation (Figure 14A), inclinometer I2 is selected as the best measurement for structural identification. Although presenting a smaller individual information entropy than other static measurements (Figure 14A), the first natural frequency is selected as the second-best measurement, showing that this dynamic measurement provides more additional information when associated with the static measurement I2 than any remaining static measurements. Then, the deflection measurement P1 is selected as the third-best measurement, showing that each type of measurements provides useful additional information. Once the measurement joint entropy is assessed, the optimal sensor configuration for the static test is directly obtained. However, the sensor-placement methodology for modal identification must be performed (Section 3.3) in order to define the optimal sensor configuration for dynamic tests.

Measurement selected	Number of measurements 1	2	3	4	5	6	7	8	9	10	11	12	13	14
M1		•	•	•	•	•	•	•	•	•	•	•	•	•
M2											•	•	•	•
M3													•	•
M4				•	•	•	•	•	•	•	•	•	•	•
M5							•	•	•	•	•	•	•	•
M6												•	•	•
M7						•	•	•	•	•	•	•	•	•
M8								•	•	•	•	•	•	•
P1			•	•	•	•	•	•	•	•	•	•	•	•
P2														•
P3										•	•	•	•	•
P4									•	•	•	•	•	•
I1					•	•	•	•	•	•	•	•	•	•
I2	•	•	•	•	•	•	•	•	•	•	•	•	•	•

Figure 15 Measurement ranking for measurement-system design including static and dynamic tests, where Mi are modes, Pi deflection-target and Ii inclinometer locations.

5.5.2 Sensor-placement for modal identification

Once the expected information gain of each mode shape is quantified, the same procedure as presented in Section 5.4.2 is performed to obtain the dynamic measurement system. Compared with the previous section, the main difference is that the importance-factor matrix is modified with the new quantification of expected modal information gain from the joint-entropy assessment of both tests (Figure 14B).

The important-factor evaluation for both static and dynamic measurements is compared in terms of objective-function evaluation, sensor-location ranking and information-gain metrics to the dynamic only importance-factor evaluation and the traditional approach where mode shapes are taken to be equally important.

Figure 16 presents the normalized objective-function evaluation ($\widehat{\mathrm{tr}}(\overline{\mathbf{Q}})$) with respect to the number of accelerometers. Results show that the new importance-factor evaluation outperforms the scenario with equal importance factors. This result confirms previous observations (Section 5.4.2)where scenarios involving various importance factors lead to larger objective-function evaluations than the traditional approach where mode shapes are taken as equally important for structural identification.

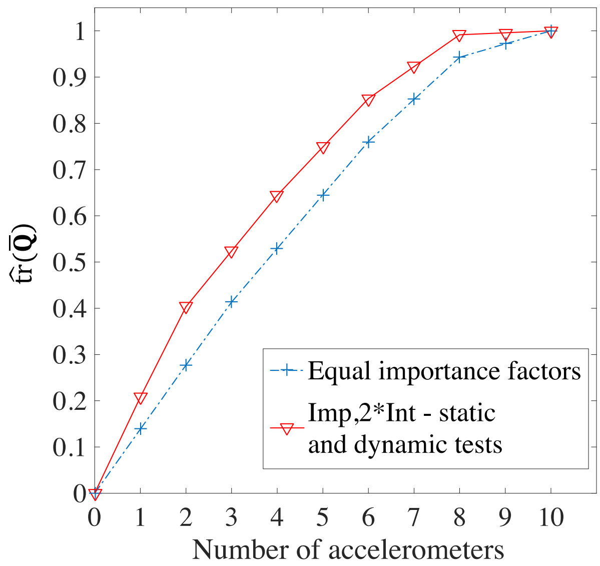

Figure 16 Normalized trace of modified Fisher Information Matrix ($\bar{\mathbf{Q}}$) for importance-factor scenarios as function of number of accelerometers.

Figure 17 presents sensor-location ranking for the three impact-factor scenarios for the five first sensor locations selected. Globally, sensor-location rankings of importance-factor scenarios differ, showing that the choice of importance factors significantly influences sensor-location evaluations. When importance-factor evaluations include dynamic tests individually and static and dynamic tests, the first two sensor locations selected remain the same. However, from the third sensor-location selection, sensor-location selections differ, showing that small difference in importance factor may significantly influence sensor-location selections.

A)	Equal importance factors				
Sensor	Number of sensors in sensor config.				
selected	1	2	3	4	5
A1					
A2				•	•
A3					
A4					
A5					•
A6					
A7	•	•	•	•	•
A8			•	•	•
A9					
A10		•	•	•	•

B)	$I_{mp,2}$ * I_{nt} - Dynamic test only				
Sensor	Number of sensors in sensor config.				
selected	1	2	3	4	5
A1					
A2					
A3	•	•	•	•	•
A4					
A5					•
A6					
A7			•	•	•
A8		•	•	•	•
A9					
A10				•	•

C)	$I_{mp,2}$ * I_{nt} - Static + dynamic tests				
Sensor	Number of sensors in sensor config.				
selected	1	2	3	4	5
A1					
A2			•	•	•
A3	•	•	•	•	•
A4					
A5				•	•
A6					
A7					•
A8		•	•	•	•
A9					
A10					

Figure 17 Accelerometer-location (Ai) ranking for importance-factor scenarios of mode-shape matrix. A) Scenario of equal importance of mode shapes; B) Importance scenario of $\mathbf{I}_{mp,2}$*$\mathbf{I}_{nt}$ using the joint entropy of dynamic test only; C) Importance scenario of $\mathbf{I}_{mp,2}$*$\mathbf{I}_{nt}$ using the joint entropy for static and dynamic tests.

Figure 18 presents MI and QRD metrics for modal identification for the two impact-factor scenarios with respect to the number of accelerometers. The missing information gain metric

MI (Figure 18A) shows a better performance if importance factors are used. As all mode-shapes are useful even if static measurements are added to dynamic measurements (Figure 14B), the number of sensors needed to identify correctly all mode shape remains constant. Therefore, the recommended number of accelerometers (i.e. 6 to 9) remains similar to the previous analysis for dynamic load tests only (Section 5.4.2.3). The main difference is that accelerometer locations are modified since the sensor-location ranking is re-evaluated (Figure 17).

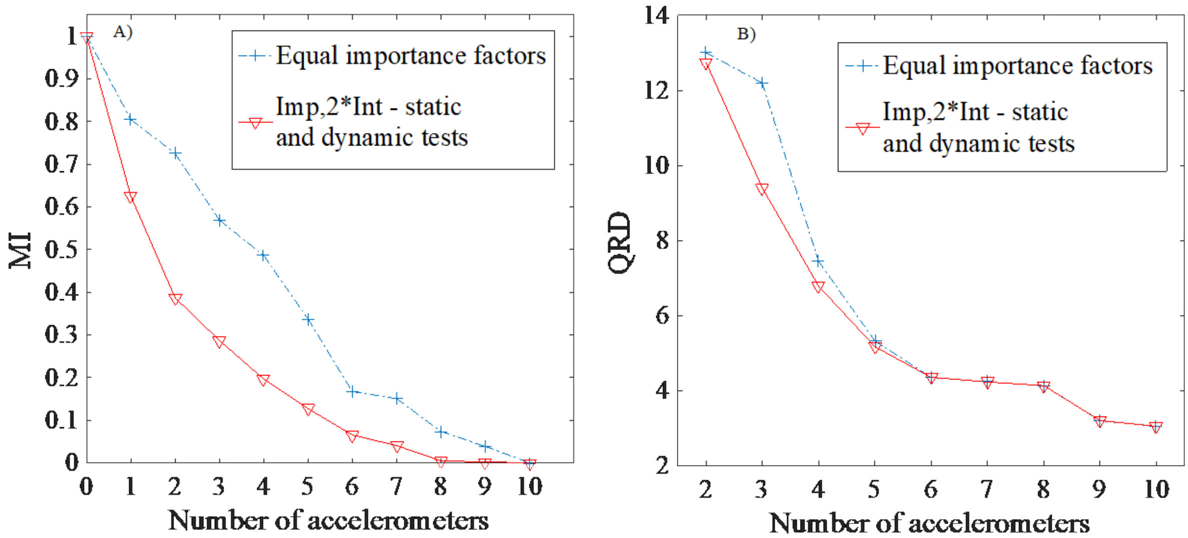

Figure 18 A) Missing-information metric for importance-factor scenarios as function of number of accelerometers; B) QR-decomposition metric for importance-factor scenarios as function of number of accelerometers.

5.6 Result corroboration using measurements taken from a full-scale bridge

As mentioned in Section 5.1, this study is performed after the bridge was monitored. Performance of both static and dynamic measurements is assessed based on their ability to falsify model instances. In the joint-entropy assessment of static and dynamic measurements (Figure 14, Section 5.5.1), both tests are expected to provide unique information. Figure 19 presents candidate-model-set domains obtained using static and dynamic measurements independently and static and dynamic measurements combined. Results are taken from Cao et al. [47], where a surrogate model was built to generate more initial model instances in order to better cover the model-parameter domain of candidate-model sets. Static measurements (i.e. all inclinometers and deflection targets) are useful to reduce parameter ranges for the first and third parameters (E_{con} and K_{rot}). They cannot help in the identification of the second and the fourth parameters (K_{long} and ρ_{con}). Figure 19 presents the boundaries of the parameter domains.

Among static candidate models, large parameter values of E_{con} are associated with small values of K_{Long} and inversely.

Dynamic measurements (i.e. all natural frequencies) reduce parameter ranges for the first and the fourth parameters (E_{con} and ρ_{con}), but have no impact on parameter ranges for the second and third parameters (K_{long} and K_{rot}). When static and dynamic measurements are combined, all model-parameter ranges are significantly reduced, showing a good structural identification even for the second model parameter K_{long} that is not well identified when static and dynamic tests are used independently. This shows that both tests provide useful information and when they are combined, the information gained is significantly increased. This result using bridge measurements corroborates the expected performance of static and dynamic tests presented in the sensor-placement study.

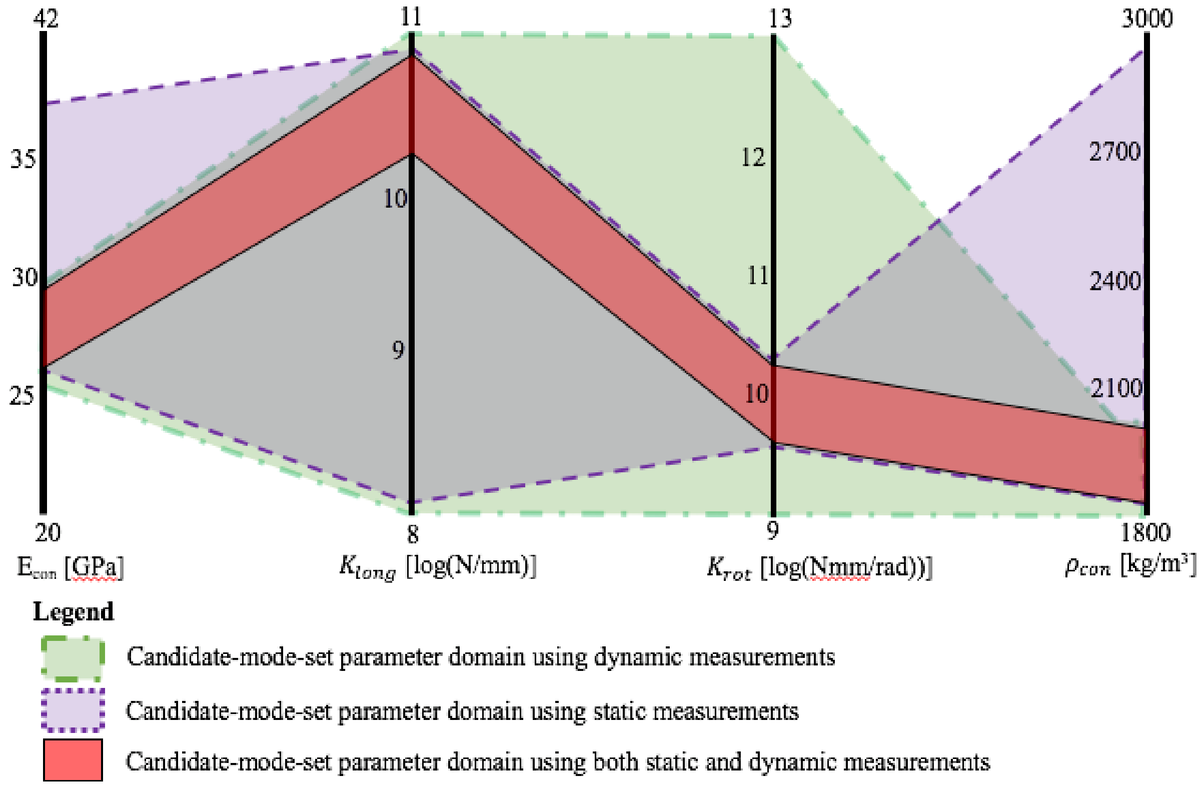

Figure 19 Parallel-axis plot of candidate-model-set parameter domain using static measurements; dynamic measurements; static and dynamic measurements. Adapted from [47].

In the study of Cao et al. [47], 10 accelerometers were used to evaluate real bridge modal frequencies and then the model-falsification process was performed. However, the present study suggests that only six accelerometers provide significant new information, while the remaining four present a large amount of redundant information (Section 5.5). Natural-frequency evaluations using only the six best accelerometers are performed again and results in terms of parameter ranges of candidate model sets are presented in Table 4. When using the six best accelerometers instead of all accelerometers, small differences of parameter identification are revealed for E_{con} and ρ_{con}. However, when static and dynamic measurements are combined, changes in parameter-identification ranges are more important. Using the accelerometer subset obtained with the proposed methodology does not significantly influence the candidate-model set. Therefore, results show that the proposed methodology help reduce the number of sensors without compromising the performance of structural identification.

Table 4 Identification of parameter ranges using static measurements; dynamic measurements and static and dynamic measurements. Adapted from [47].

Load testing	E_{con} [Gpa]		K_{long} [log(N/mm)]		K_{rot} [log(Nmm/rad)]		ρ_{con} [kg/m^3]	
	min	max	min	max	min	max	min	max
Static only	28.1	37.0	9.2	12.8	8.4	8.9	1800	2900
Dynamic only – All accelerometers	26.7	29.9	9.0	13.0	8.0	11.0	1800	1950
Dynamic only – 6 best accelerometers	26.2	29.7	9.0	13.0	8.0	11.0	1800	2000
Static + Dynamic – All accelerometers	28.1	29.9	12.2	12.8	8.5	8.9	1800	1950
Static + Dynamic – 6 best accelerometers	28.1	29.7	12.2	12.8	8.5	8.9	1800	2000

Additionally, information-gain metrics (Figure 18) provide information related to the minimum number of sensors to accurately identify mode shapes. Information-gain metrics show that 6 and 9 accelerometers are required for two scenarios of sensor placement respectively: $\mathbf{I_{mp,2}*I_{nt}}$ and the equal importance factor. Figure 20 presents the error in the measured natural frequency of the first mode with respect to the number of accelerometers. The error in measured natural frequencies is evaluated as the difference between the frequency obtained when a subset of sensors is used $\tilde{f}$ with the frequency obtained considering all accelerometers f. Results are normalized using f and are compared for sensor configurations selected by both scenarios (Figure 17). The error in frequency estimation decreases while increasing the number of accelerometers for both scenarios. Sensor configurations selected by the $\mathbf{I_{mp,2}*I_{nt}}$ scenario provide better approximation of the first natural frequency than the equal-importance scenario. As the first mode provides the largest increase of joint entropy (Figure 14), this result demonstrates that the $\mathbf{I_{mp,2}*I_{nt}}$ scenario prioritizes sensor locations to identify useful modes.

Additionally, results show the $\mathbf{I_{mp,2}}$*$\mathbf{I_{nt}}$ scenario requires at least 5 sensors to approximate accurately the natural frequency while the equal-importance-factors scenario requires 8 sensors, corroborating results of information-gain metrics. Globally, results show that the expected performance of accelerometers of this study is corroborated using field measurements [47].

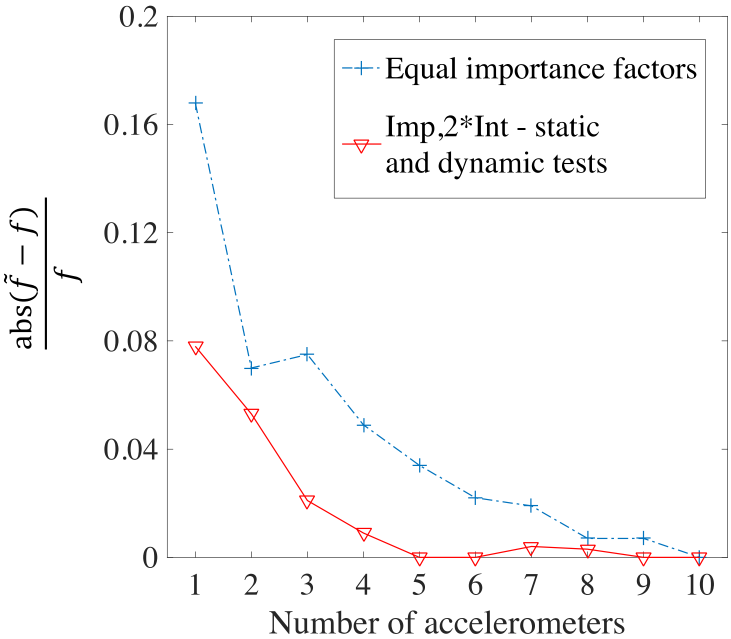

Figure 20 Error in the measured natural frequency for the first mode shape as function of the number of accelerometers.

6 Discussion

The following limitations of the work are recognized. First, the objective function for modal identification in the dynamic methodology employs only information on the diagonal of the FIM to select sensor locations. This choice was motivated by the fact that the number of sensors was low compared with the number of mode shapes. Therefore, the determinant of the FIM equals zero and thus cannot be used as sensor-placement objective function. When the number of sensors is larger than the number of useful mode shapes, the determinant of the FIM could be a more appropriate objective function for sensor placement (Section 3.3.3). The determinant involves complete information contents of the FIM, while the trace involves only information on the diagonal of the FIM.

Greedy search is used as optimization algorithm to reduce the computational time. However, it may lead to suboptimal sensor configurations, especially when there are few sensors. In order to combine information of both static and dynamic load testing, joint-entropy evaluations of respective measurements need to be compared. This implies that the same initial model sets of model-parameter values are used. Thus, a single model class is used and it should include all model parameters influencing both static and dynamic predictions.

Selections of mode shapes and possible sensor locations are treated as engineering decisions. However, it is recommended to include large sets in order to find optimal measurement systems. Sensor locations that were involved in the previous study [47] are employed in order to compare the expected performance of both static and dynamic tests with reality. Results of the sensor-placement study are corroborated using real measurements. However, this is not a firm result validation since sensor-placement strategies provide only a statistical advantage in terms of expected performance. A large sample of case studies must be compared in order to achieve result validation that would justify generalization of any sensor-placement methodology. To validate a sensor configuration for modal identification, real mode-shape vectors should be compared using a complete set of sensors and using a subset with only important sensor locations.

The proposed measurement-system design framework takes into account only information-gain metrics. In addition to the information gain, characteristics such as monitoring costs, sensor installation and robustness of information gain to sensor failure should be evaluated to design an optimal measurement system. Additionally, the criterion-weighting preferences of asset managers must be supported. A framework using a multi-criteria-decision-analysis approach and five performance metrics has recently been proposed in [48].

The success of any sensor-placement methodology depends directly on the quality of the numerical behavior model that is used to obtain predictions. Before installing the sensor configuration, the material constants and reliability of model assumptions should be verified using visual inspection and non-destructive testing methods.

The information collected through load testing in the elastic domain is used to update the structural behavior at limit-state conditions. If the critical limit state is the ultimate limit state and the response is non-linear behavior that is difficult to model, as would be expected for a reinforced concrete beams in bending, structural-identification methodologies may provide limited information since the updated-parameter sensitivity is low. Further research is also needed to recommend appropriate values of numerical-simulation uncertainties [49]. In such situations, while the interest of measurement-system-design methodologies is reduced, methodologies remain valid.

7 Conclusions

A well-designed measurement system enhances structural identification and reserve-capacity assessment. The following are the specific conclusions of the study:

- The measurement-system-design methodology that is proposed in this paper for dynamic load tests supports asset managers for tasks of finding optimal sensor configurations and quantifying expected information gain of natural frequencies for structural identification.
- Taking into account importance and identifiability matrices helps prioritize sensor locations in the effective independence method (EFI) for modal identification without requiring additional uncertainty information.
- Combining information from measurement-system-design methodologies for static and dynamic load testing leads to measurement systems where the redundancy of information gain is minimized in a unique way.

Future work will involve quantifying the expected influence of monitoring information gain for both static and dynamic load testing to assess reserve capacity.

Acknowledgements

This research was conducted at the Future Cities Laboratory at the Singapore-ETH Centre (SEC). The SEC was established as a collaboration between ETH Zurich and National Research Foundation (NRF) Singapore (FI 370074011) under the auspices of the NRF's Campus for Research Excellence and Technological Enterprise (CREATE) programme. The authors would like to acknowledge the support of the Land Transport Authority of Singapore (LTA) for the case study. Additionally, the authors are thankful to A. Costa, W. Cao and Y. Reuland for their valuable input.

Conflict of interest

The authors declare that they have no conflict of interest.

References

[1] World Economic Forum, "Shaping the Future of Construction, A Breakthrough in Mindset and Technology," 2016.

[2] F. Catbas, T. Kijewski-Correa, T. Lynn, and A. Aktan, *Structural identification of constructed systems*. American Society of Civil Engineers, 2013.

[3] J. M. W. Brownjohn, A. De Stefano, Y.-L. Xu, H. Wenzel, and A. E. Aktan, "Vibration-based monitoring of civil infrastructure: challenges and successes," *J. Civ. Struct. Health Monit.*, vol. 1, no. 3, pp. 79–95, Dec. 2011.

[4] I. F. C. Smith, "Studies of Sensor Data interpretation for Asset Management of the Built environment," *Front. Built Environ.*, vol. 2, pp. 2–8, 2016.

[5] J. L. Beck and L. S. Katafygiotis, "Updating models and their uncertainties. I: Bayesian statistical framework," *J. Eng. Mech.*, vol. 124, no. 4, pp. 455–461, 1998.

[6] L. S. Katafygiotis and J. L. Beck, "Updating models and their uncertainties. II: Model identifiability," *J. Eng. Mech.*, vol. 124, no. 4, pp. 463–467, 1998.

[7] H.-F. Lam, J. Yang, and S.-K. Au, "Bayesian model updating of a coupled-slab system using field test data utilizing an enhanced Markov chain Monte Carlo simulation algorithm," *Eng. Struct.*, vol. 102, pp. 144–155, Nov. 2015.

[8] R. Pasquier, J.-A. Goulet, C. Acevedo, and I. F. C. Smith, "Improving fatigue evaluations of structures using in-service behavior measurement data," *J. Bridge Eng.*, vol. 19, no. 11, p. 04014045, 2014.

[9] M. C. Vuran, Ö. B. Akan, and I. F. Akyildiz, "Spatio-temporal correlation: theory and applications for wireless sensor networks," *Comput. Netw.*, vol. 45, no. 3, pp. 245–259, Jun. 2004.

[10] E. Simoen, C. Papadimitriou, and G. Lombaert, "On prediction error correlation in Bayesian model updating," *J. Sound Vib.*, vol. 332, no. 18, pp. 4136–4152, 2013.

[11] S. G. S. Pai, A. Nussbaumer, and I. F. C. Smith, "Comparing Structural Identification Methodologies for Fatigue Life Prediction of a Highway Bridge," *Front. Built Environ.*, vol. 3, 2018.

[12] J.-A. Goulet and I. F. C. Smith, "Structural identification with systematic errors and unknown uncertainty dependencies," *Comput. Struct.*, vol. 128, pp. 251–258, 2013.

[13] R. Pasquier and I. F. C. Smith, "Robust system identification and model predictions in the presence of systematic uncertainty," *Adv. Eng. Inform.*, vol. 29, no. 4, pp. 1096–1109, 2015.

[14] M. Proverbio, D. G. Vernay, and I. F. C. Smith, "Population-based structural identification for reserve-capacity assessment of existing bridges," *J. Civ. Struct. Health Monit.*, pp. 1–20, Apr. 2018.

[15] D. G. Vernay, F.-X. Favre, and I. F. C. Smith, "Robust model updating methodology for estimating worst-case load capacity of existing bridges," *J. Civ. Struct. Health Monit.*, pp. 1–18, 2018.

[16] C. Argyris, C. Papadimitriou, and P. Panetsos, "Bayesian Optimal Sensor Placement for Modal Identification of Civil Infrastructures," *J. Smart Cities*, vol. 2, no. 2, 2017.

[17] R. Pasquier, J.-A. Goulet, and I. F. C. Smith, "Measurement system design for civil infrastructure using expected utility," *Adv. Eng. Inform.*, vol. 32, pp. 40–51, 2017.

[18] H. Schlune, M. Plos, and K. Gylltoft, "Improved bridge evaluation through finite element model updating using static and dynamic measurements," *Eng. Struct.*, vol. 31, no. 7, pp. 1477–1485, Jul. 2009.

[19] J.-A. Goulet and I. F. C. Smith, "Performance-driven measurement system design for structural identification," *J. Comput. Civ. Eng.*, vol. 27, no. 4, pp. 427–436, 2012.

[20] H. M. Chow, H. F. Lam, T. Yin, and S. K. Au, "Optimal sensor configuration of a typical transmission tower for the purpose of structural model updating," *Struct. Control Health Monit.*, vol. 18, no. 3, pp. 305–320, Apr. 2011.

[21] D. C. Kammer, "Sensor set expansion for modal vibration testing," *Mech. Syst. Signal Process.*, vol. 19, no. 4, pp. 700–713, 2005.

[22] C. Papadimitriou, J. L. Beck, and S.-K. Au, “Entropy-based optimal sensor location for structural model updating,” *J. Vib. Control*, vol. 6, no. 5, pp. 781–800, 2000.
[23] C. Papadimitriou, “Optimal sensor placement methodology for parametric identification of structural systems,” *J. Sound Vib.*, vol. 278, no. 4, pp. 923–947, 2004.
[24] Y. Robert-Nicoud, B. Raphael, and I. F. C. Smith, “Configuration of measurement systems using Shannon’s entropy function,” *Comput. Struct.*, vol. 83, no. 8, pp. 599–612, 2005.
[25] P. Kripakaran and I. F. C. Smith, “Configuring and enhancing measurement systems for damage identification,” *Adv. Eng. Inform.*, vol. 23, no. 4, pp. 424–432, 2009.
[26] K. Yuen and S. Kuok, “Efficient Bayesian sensor placement algorithm for structural identification: a general approach for multi-type sensory systems,” *Earthq. Eng. Struct. Dyn.*, vol. 44, no. 5, pp. 757–774, 2015.
[27] C. Papadimitriou and G. Lombaert, “The effect of prediction error correlation on optimal sensor placement in structural dynamics,” *Mech. Syst. Signal Process.*, vol. 28, pp. 105–127, 2012.
[28] M. Papadopoulou, B. Raphael, I. F. C. Smith, and C. Sekhar, “Hierarchical sensor placement using joint entropy and the effect of modeling error,” *Entropy*, vol. 16, no. 9, pp. 5078–5101, 2014.
[29] M. Papadopoulou, B. Raphael, I. F. C. Smith, and C. Sekhar, “Optimal sensor placement for time-dependent systems: Application to wind studies around buildings,” *J. Comput. Civ. Eng.*, vol. 30, no. 2, p. 04015024, 2015.
[30] N. J. Bertola, M. Papadopoulou, D. G. Vernay, and I. F. C. Smith, “Optimal multi-type sensor placement for structural identification by static-load testing,” *Sensors*, vol. 17, no. 12, p. 2904, 2017.
[31] P. C. Shah and F. E. Udwadia, “A Methodology for Optimal Sensor Locations for Identification of Dynamic Systems,” *J. Appl. Mech.*, vol. 45, no. 1, pp. 188–196, Mar. 1978.
[32] M. Salama, T. Rosa, and J. Garba, “Optimal placement of excitations and sensors for verification of large dynamical systems,” in *28th Structures, Structural Dynamics and Materials Conference*, American Institute of Aeronautics and Astronautics, 1987, pp. 1024–1030.
[33] D. C. Kammer, “Sensor placement for on-orbit modal identification and correlation of large space structures,” *J. Guid. Control Dyn.*, vol. 14, no. 2, pp. 251–259, Mar. 1991.
[34] T. G. Carne and C. Dohrmann, “A modal test design strategy for model correlation,” presented at the Proceedings-Spie The International Society For Optical Engineering, 1995, pp. 927–927.
[35] C. Schedlinski and M. Link, “An approach to optimal pick-up and exciter placement,” in *Proceedings-SPIE the international society for optical engineering*, 1996, pp. 376–382.
[36] C. Stephan, “Sensor placement for modal identification,” *Mech. Syst. Signal Process.*, vol. 27, pp. 461–470, 2012.
[37] T. Yi, H. Li, and M. Gu, “Optimal sensor placement for structural health monitoring based on multiple optimization strategies,” *Struct. Des. Tall Spec. Build.*, vol. 20, no. 7, pp. 881–900, 2011.
[38] G. C. Marano, G. Monti, and G. Quaranta, “Comparison of different optimum criteria for sensor placement in lattice towers,” *Struct. Des. Tall Spec. Build.*, vol. 20, no. 8, pp. 1048–1056, 2011.
[39] C. Leyder, V. Dertimanis, A. Frangi, E. Chatzi, and G. Lombaert, “Optimal sensor placement methods and metrics – comparison and implementation on a timber frame structure,” *Struct. Infrastruct. Eng.*, vol. 14, no. 7, pp. 997–1010, Jul. 2018.

[40] M. Meo and G. Zumpano, “On the optimal sensor placement techniques for a bridge structure,” *Eng. Struct.*, vol. 27, no. 10, pp. 1488–1497, Aug. 2005.

[41] J.-A. Goulet, M. Texier, C. Michel, I. F. C. Smith, and L. Chouinard, “Quantifying the effects of modeling simplifications for structural identification of bridges,” *J. Bridge Eng.*, vol. 19, no. 1, pp. 59–71, 2013.

[42] Y. Robert-Nicoud, B. Raphael, O. Burdet, and I. F. C. Smith, “Model identification of bridges using measurement data,” *Comput. Civ. Infrastruct. Eng.*, vol. 20, no. 2, pp. 118–131, 2005.

[43] Z. Šidák, “Rectangular confidence regions for the means of multivariate normal distributions,” *J. Am. Stat. Assoc.*, vol. 62, no. 318, pp. 626–633, 1967.

[44] Y. Robert-Nicoud, B. Raphael, and I. F. C. Smith, “System identification through model composition and stochastic search,” *J. Comput. Civ. Eng.*, vol. 19, no. 3, pp. 239–247, 2005.

[45] R. Pasquier and I. F. C. Smith, “Iterative structural identification framework for evaluation of existing structures,” *Eng. Struct.*, vol. 106, pp. 179–194, 2016.

[46] J.-A. Goulet, “Probabilistic model falsification for infrastructure diagnosis,” EPFL, IMAC, Thesis no 5417, 2012.

[47] W.-J. Cao, C. G. Koh, and I. F. C. Smith, “Enhancing static-load-test identification of bridges using dynamic data,” *Eng. Struct.*, vol. 186, pp. 410–420, 2019.

[48] N. J. Bertola, M. Cinelli, S. Casset, S. Corrente, and I. F. C. Smith, “A multi-criteria decision framework to support measurement-system design for bridge load testing,” *Adv. Eng. Inform.*, vol. 39, pp. 186–202, Jan. 2019.

[49] H. Schlune, M. Plos, and K. Gylltoft, “Safety formats for non-linear analysis of concrete structures,” *Mag. Concr. Res.*, vol. 64, no. 7, pp. 563–574, 2012.